Life history diversity and signals of trade-offs in a large group of chloroviruses

Eva J.P. Lievens, Irina Agarkova, David D. Dunigan, James L. Van Etten, and Lutz Becks

Abstract

Microbial viruses affect the ecology and evolution of every environment on earth. Although these effects can play out on a grand scale, to understand them we need to zoom in to virus' life cycle traits. The values of these traits determine a virus' effect on the host population, the trait diversity provides the material for natural selection, and trade-offs between the traits are expected to constrain virus' evolutionary potential. However, due to the difficulty involved in measuring viral life history phenotypes, there are not many studies that characterize their diversity within clades of viruses. In this study, we quantified the life history of 35 chloroviruses from three host range groups (NC64A, Osy, and SAG viruses). We developed methods to efficiently measure adsorption rate, depolarization probability, lysis probability, lysis time, burst size, specific infectivity, and decay. The trait estimates varied between 5 and 75-fold across all the virus strains, with most traits varying substantially both within and across groups. We then used our largest virus group, the NC64A viruses (n = 20), to look for correlations that could signal trade-offs between traits. We found that viruses with high depolarization probabilities also had higher burst sizes, but lower lysis probabilities once depolarized. These correlations were strong, but their mechanistic underpinnings are unclear. We also found a strong correlation between growth rate and survival in the NC64A viruses. Finally, we discovered biphasic or 'tailing' decay in all the chlorovirus groups. The nature and diversity of these traits has large implications for the ecology and evolutionary potential of the chloroviruses, and confirm the importance of studying viral life cycle traits.

Introduction

Microbial viruses play an essential role in the ecology and evolution of every environment on earth: they control host populations, change species communities and nutrient flow, and prompt evolutionary change (Suttle, 2007; Middelboe *et al.*, 2008; Williamson *et al.*, 2017). To understand these effects, it is essential to study viral life histories. Viral life histories are made up of life cycle or 'performance' traits such as adsorption rate, lysogeny probability, burst size, and decay rate (performance *sensu* DeLong *et al.*, 2022). The values of these traits determine a virus' population dynamics and ability to suppress the host population, and thus its impact on the broader ecosystem (Weitz, 2016; Horas *et al.*, 2018). The variation in life cycle traits is also crucial, as diverse phenotypes provide material for natural selection. Life history traits are also likely to be subject to trade-offs that constrain the evolutionary potential (Stearns, 1989; Goldhill & Turner, 2014; Keen, 2014), and whose effects can feed back to the community level (Record *et al.*, 2016).

Despite the importance of life history traits, there are not many studies that characterize their diversity within viral clades. Measuring life cycle traits requires either microscopic resolution (e.g. Timm & Yin, 2012; Vincent *et al.*, 2021; DeLong *et al.*, 2022), which is challenging, or tracking virus concentrations over time (Hiatt, 1964; Hyman & Abedon, 2009), which is labor-intensive when applied to multiple strains. Most studies of multiple (> 3) viruses analyze the diversity within a host species (Baudoux & Brussaard, 2005; De Paepe & Taddei, 2006; Stenholm *et al.*, 2008; Kahn Mirzaei & Nilsson, 2015), or assemble information within viral ecotypes (Kukkaro & Bamford, 2009; Mojica & Brussaard, 2014; Jurczak-Kurek *et al.*, 2016; Edwards & Steward, 2018), and most of these focus on a subset of the life cycle traits (an excellent exception is Ceyssens *et al.*, 2011). As a result, there is a growing information gap between our understanding of viral genetic diversity and the phenotypes

that are necessary to parameterize epidemiological models and predict evolutionary responses (DeLong *et al.*, 2022).

In this study, we quantified the life history of a large group of chloroviruses. Chloroviruses (family *Phycodnaviridae*, genus *Chlorovirus*) are dsDNA viruses that infect unicellular 'chlorella-like' green algae (Van Etten *et al.*, 2020). They have a lytic life cycle (Fig. 1). Briefly, upon adsorption (which is nigh-on unlimited per host cell, Meints *et al.*, 1988) the virus digests a hole in the host cell wall through which the host and virion membranes fuse, forming a membrane-lined channel (Thiel *et al.*, 2010; Agarkova *et al.*, 2021). Virion-associated proteins then depolarize the host cell plasma membrane, allowing viral DNA and proteins to enter (Thiel *et al.*, 2010; Milrot *et al.*, 2017). The depolarization prevents infection by other chloroviruses (mutual exclusion, Greiner *et al.*, 2009). Viral DNA is replicated in or near the nucleus, packaged into capsids in the cytoplasm, and eventually mature virions escape by lysis (Milrot *et al.*, 2017). Virions are large (~190 nm, Yan *et al.*, 2000; Quispe *et al.*, 2017) and their decay is temperature-dependent (Van Etten *et al.*, 1983; Agarkova *et al.*, 2014). The chloroviruses are known to vary in genome content and plaque size (Van Etten *et al.*, 1988; Rodrigues *et al.*, 2022), for example, but the life cycle traits have almost exclusively been measured in the type strain PBCV-1 (exceptions: Van Etten *et al.*, 1988; Greiner *et al.*, 2009; Quispe *et al.*, 2017; Schiano di Visconte *et al.*, 2022).

We developed methods that combine flow cytometry, classic kinetic assays, and statistical modeling to overcome the challenges of measuring viral life cycles. We used these methods to quantify the full life cycle of 35 chlorovirus strains (Fig. 1), explored their phenotypic diversity, and looked for evidence of trade-offs between traits.

Methods

We measured the life history traits of 35 chlorovirus strains using new versions of the classic one-step growth and persistence assays. The modified assays are higher throughput and allow quantification of the entire life cycle (Fig. 1); they rely on the distinction between virions and infective virions. In what follows, viruses are described as 'virions', 'depolarizing-capable virions', or 'infective virions', and we use the terms 'multiplicity of particles (MOP)', 'multiplicity of adsorption (MOA)', and 'multiplicity of infection (MOI)'. These terms are defined for our purposes in Table 1.

Viruses, algae, and experimental conditions

The genus *Chlorovirus* is divided into four virus groups, which are defined by their host range and phylogeny (Van Etten *et al.*, 2020). We used viruses from three groups: NC64A viruses, which infect the ciliate endosymbionts *Chlorella variabilis* NC64A and *C. variabilis* Syngen 2-3, Only Syngen viruses (Osy viruses), which infect *C. variabilis* Syngen 2-3 but not *C. variabilis* NC64A, and SAG viruses, which infect the heliozoon endosymbiont *Chlorella heliozoae* SAG 3.83. All of the described procedures took place in the type hosts (e.g. the SAG viruses were amplified and assayed in SAG 3.83).

The algal strains NC64A, Syngen 2-3, and SAG 3.83 were stored on agar slants at 4°C and inoculated into liquid medium before use. We used a modified version of BBM (Nichols & Bold, 1965), with ammonium chloride substituted for sodium nitrate as a nitrogen source and twice the concentration of trace element solution 4 (first used by Frickel *et al.*, 2016). We keep the abbreviation BBM in order to distinguish our medium from the enriched "MBBM" typically used in this model system (e.g. Van Etten *et al.*, 1983). Growth was on a shaker under the standard conditions (see below). The algae used for the described assays were in late exponential phase (~$1x10^6$ algae/ml in this medium).

We phenotyped 20 NC64A viruses, 7 Osy viruses, and 8 SAG viruses (Table 2). These strains were isolated from natural ponds or streams around the world between 1981 and 2017, and have been maintained as part of a stock collection since then. Lysates were stored at 4°C. Before starting the assays, we refreshed and amplified the virus stocks: 0.5ml of the original lysate was inoculated into 10ml of $2x10^6$ algae/ml solution, left on a shaker under the standard conditions (see below) until they lysed (24h or 48h), and syringe-filtered through 0.2µm. The resulting filtrates were stored at 4°C and their virion concentration was measured by flow cytometry (see below). The filtrates with insufficient virion concentrations were given one more round of this amplification treatment.

Algal growth and virus replication took place under the 'standard conditions': 20°C and constant light. Unless otherwise specified, 'shaker' refers to an orbital shaker with diameter 10mm and frequency 120rpm. The term 'culture plates' always refers to 96-well flat-bottomed tissue culture plates (Techno Plastic Products, CH); 'deep well plates' always refers to 96-well 2.2ml PP deep well plates (VWR International, USA). Any 4°C storage was also dark storage.

Virion quantification with flow cytometry

To quantify virions, we used a flow cytometry protocol based on Brussaard et al. (2004) and Wen et al. (2004). Our version does not require fixation and can handle up to 96 samples at a time with 97-99% repeatability (data not shown). Briefly, virus samples were mixed with SYBR Green I stain (Merck, Germany) and Tris-EDTA buffer in a PCR plate, to a final volume of 150µl and a final SYBR Green concentration of 0.5X. Depending on the expected virion concentration, 7.5 or 30µl of virus sample was used. The samples were heated to 80°C for 10min, allowed to cool for 15min, and then analyzed on a flow cytometer. We use a BD FACSVerse (BD Biosciences, USA), which has an automated loader and records the analyzed volume. Each sample was run for 30s (40-50µl), and the virion population was identified based on its side scatter and green fluorescence. A detailed protocol is provided in Supp. Method 1.

Modified one-step growth (mOSG) assay

In a classic one-step growth assay, viruses and hosts are mixed at a given MOI and allowed to adsorb for a short time. The solutions are then diluted to synchronize the infections, and the increase in plaque-forming units is used to calculate the latent period and burst size (Hyman & Abedon, 2009). Our mOSG assay followed the same principle of adsorption, dilution, and quantification, but with two key differences. First, we worked with virions, not infective virions: we inoculated based on MOP, and measured the increase in virion concentration. Second, we varied the MOP across replicates. These two differences allowed us to calculate the adsorption constant (k) and depolarization probability (d) in addition to the latent period ($\mu_l \pm \sigma_l$) and burst size (b_d) (Fig. 1). The methods are related to those presented by Brown & Bidle (2014) and Taylor et al. (2018), but combine the advantages of both.

The mOSG assay is represented schematically for one virus strain in Fig. 2. We combined algae and viruses in a set of culture plates. Each well contained 0.1ml solution with $1.5*10^7$ algae/ml and either MOP 0.5, 1, 2, 5, or 10 of a given virus filtrate (MOP 20 was included for a few strains where there was room on the plates). The virus volumes were pipetted independently, so that the different MOPs also functioned as statistically independent replicates. Virus-free controls were present on every plate. Immediately after combining algae and viruses, the culture plates were shaken at high speed for 15min to induce adsorption (1200rpm on a microplate shaker with orbital diameter

1mm[1]). The solutions were then diluted 1000-fold[2] into nine sets of deep well plates (2µl solution + 1998µl BBM) to synchronize infections. The deep well plates were sealed with transparent foil and left under the standard conditions (see above); they were flipped every hour to prevent sedimentation[3]. At time points 0h, 2h, 4h, …, 16h after dilution, we collected a set of deep well plates for sampling. Sampling was done as follows: deep well plates were centrifuged for 15min at 2000g to separate virions from algae; supernatants (containing virions) were transferred into culture plates, sealed, and stored at 4°C. The virion concentration in the supernatants was quantified by flow cytometry within one week after sampling. Because one set of deep well plates was prepared for every sampling time point, the time points were statistically independent of each other. We also prepared one deep well plate containing a 1:10000 dilution, whose purpose was to check for signals of secondary infection in the growth curves (not shown in Fig. 2; see Supp. Fig. 1). This plate was sampled after 16h.

The data we collected was the concentration of virions over time after dilution; we used a non-linear least squares fitting to extract our parameters of interest. For each virus strain, we fit the free virion concentration over time $V(t)$. Virions were either leftover unadsorbed virions or newly released progeny virions, i.e.

$V(t) = \frac{V_{unadsorbed}}{\delta} + V_{progeny}$ (Eq. 1.1)

$V(t) = \frac{V_{unadsorbed}}{\delta} + \frac{A_{depolarized}}{\delta} * c * l(t) * b_c$ (Eq. 1.2)

$V(t) = \frac{1}{\delta} * (V_{unadsorbed} + A_{depolarized} * l(t) * b_d)$ (Eq. 1.3),

where δ is the dilution factor, $V_{unadsorbed}$ is the concentration of unadsorbed virions at the end of the adsorption period, $A_{depolarized}$ is the concentration of depolarized algae at the end of the adsorption period, c is the probability that a depolarized cell completes the life cycle, $l(t)$ expresses the proportion of lysed cells over time, and b_c is the average burst size per completed cell. $c * b_c$ reduces to b_d, the burst size per depolarized cell (see Fig. 1). $V_{unadsorbed}$, $A_{depolarized}$, and $l(t)$ are described in more detail below. Note that b_d is a constant, and not contingent on MOP. This assumption is based on the finding that chloroviruses mutually exclude each other through depolarization (Greiner *et al.*, 2009). Therefore, we can assume that all depolarized cells behave like cells infected by one virion, no matter how many depolarizing-capable virions are attached to them (though dual infections are possible at very high MOIs, Graves *et al.*, 2001).

$V_{unadsorbed}$ is the concentration of unadsorbed virions at the end of the 15min adsorption period. We assume that all virions can adsorb, and that they adsorb at a constant rate represented by the adsorption constant k. The concentration of unadsorbed virions is then

$V_{unadsorbed} = A_{ads} * MOP * e^{-k*A_{ads}*t_{ads}}$ (Eq. 2)

(Hyman & Abedon, 2009, eq. 18.2), where A_{ads} is the algal concentration during the adsorption period, $A_{ads} * MOP$ is the virion concentration at the start of the adsorption period, and t_{ads} is the duration of the adsorption period in minutes.

$A_{depolarized}$ is the concentration of depolarized algae at the end of the adsorption period. We assume that adsorbed virions are randomly distributed across host cells, and that depolarizing-capable and depolarizing-incapable virions adsorb at the same rate. Therefore, the average number of depolarizing-capable virions that adsorb to each cell is $d * MOA$, where *d* is the proportion of

---

[1] These conditions led to ≥ 80% adsorbed virions in preliminary tests with PBCV-1 (data not shown). Shaking at 500rpm on a standard shaker with orbital diameter 10mm also works well (data not shown).

[2] 1:100 dilutions did not prevent secondary infection (data not shown).

[3] Several mixing methods were tested; flipping was similar to mild shaking (data not shown).

depolarizing-capable virions (i.e. the depolarization probability when a virion is adsorbed). We use this as the expected number of events in a Poisson distribution:

$A_{depolarized} = A_{ads} * P_{Poisson}(\geq 1\ depolarizingcapable\ virion\ adsorbs)$ (Eq. 3.1)

$A_{depolarized} = A_{ads} * (1 - P_{Poisson}(0\ depolarizingcapable\ virions\ adsorb))$ (Eq. 3.2)$A_{depolarized} = A_{ads} * \left(1 - e^{-expected\ number\ of\ depolarizingcapable\ virions}\right) = A_{ads} * \left(1 - e^{-d*MOA}\right)$ (Eq. 3.3).

The MOA is

$MOA = \frac{V_{adsorbed}}{A_{ads}} = \frac{MOP*A_{ads}-V_{unadsorbed}}{A_{ads}} = \cdots = \left(1 - e^{-k*A_{ads}*t_{ads}}\right) * MOP$ (Eq. 4),

so the concentration of depolarized algae is

$A_{depolarized} = A_{ads} * \left(1 - e^{-d*\left(1-e^{-k*A_{ads}*t_{ads}}\right)*MOP}\right)$ (Eq. 3.4).

This non-linear function reflects the fact that maximum 100% of the algae can be depolarized. For example, when $d * MOA$ is 0.5, the fraction of depolarized algae is expected to be 39% (Eq. 3.3). Doubling the MOP (and thus doubling $d * MOA$, Eq. 4) would increase that fraction to 63%. When the initial $d * MOA$ is 5, however, the fraction of depolarized algae is already 99% and doubling it would have little effect. When combined with the constant burst size (see above), this is the key insight that allows us to disentangle burst size from depolarization probability: b_d determines the concentration of progeny virions at saturating MOPs, while d determines the saturation point.

$l(t)$, the proportion of lysed cells over time, deviates from an idealized 'step' pattern due to variation among the host cells (Rabinovitch *et al.*, 1999). Determining the precise distribution of lysis time across the host population is not trivial (e.g. Adams & Wassermann, 1956; Dennehy & Wang, 2011), but we have found the normal distribution to be an acceptable approximation for chloroviruses (methods as in Adams & Wassermann, 1956; data not shown). Thus $l(t)$ follows a Gaussian cumulative distribution function (CDF):

$l(t) = CDF(t, \mu_l, \sigma_l)$ (Eq. 5).

This function expresses the proportion of lysed cells at t hours after dilution, given a mean latent period μ_l and standard deviation σ_l.

Plugging Eq. 2, 3.4, and 5 back into Eq. 1.3, the concentration of virions in the diluted solutions is:

$V(t) = \frac{1}{\delta} * \left(A_{ads} * MOP * e^{-k*A_{ads}*t_{ads}} + A_{ads} * \left(1 - e^{-d*\left(1-e^{-k*A_{ads}*t_{ads}}\right)*MOP}\right) * CDF(t, \mu_l, \sigma_l) * b_d\right)$ (Eq. 1.4).

We fit this model to our data using nonlinear least squares fitting (function "nls" in base R version 3.6.1, R Core Team, 2014). The data was *ln*-transformed and curated before fitting: obvious outliers were removed (virion concentration implausibly high or low compared to the data for other MOPs at the same time point, or compared to other time points of that MOP), as were time points with secondary infections (aberrant 1:1000 vs. 1:10000 dilutions data at time point 16, or secondary increases at later time points for low MOPs). For the fitting, all parameters were given 0 as a lower limit. k, μ_l, σ_l, and b_d were given unrealistically high upper limits; d was given a meaningful upper limit of 1. Non-parametric bootstrapping was used to obtain 95% CIs for each parameter (function "nlsBoot" in package "nlstools", Baty *et al.*, 2015). The model was run separately for each viral strain. The model fit was assessed by visually judging the fit and distribution of residuals (Supp. Fig. 1); almost all the models fit the data very well.

We tested the repeatability of this assay in separate experiments with four MOPs (0.5, 1, 5, 10) and time points up to 14h (data not shown). Repeatabilities were 0.86 for k, 0.76 for d, 0.86 for μ_l, 0.45 for σ_l, and 0.64 for b_d (*n* = 10, 16, 8, 8, and 16 strains, respectively, each strain tested twice; calculated following Nakagawa & Schielzeth, 2010). When an effect of the testing day was included

to account for environmental variation, repeatability increased to 0.94 for μ_l, 0.55 for σ_l, and 0.82 for b_d. Note that we used more MOPs, more time points, and a single testing day in this mOSG assay, so our power was certainly higher.

Modified persistence (mP) assay

A classic persistence (also called 'survival', or conversely 'inactivation' or 'decay') assay exposes a virus solution to an environment and measures the decline in infective virions over time. At each time point, the concentration of infective virions is estimated via serial dilution methods, e.g. plaque or most probable number assays (e.g. Suttle & Chan, 1994; De Paepe & Taddei, 2006). In contrast, our mP assay started with solutions with known virion concentrations. We then measured the initial concentration and decline of infective virions, allowing us to estimate the initial frequency of infective virions (*s*, the specific infectivity) and their decay rate (*m*) (Fig. 1). The data also supported the existence of an additional trait, the robust fraction (*r*, see below) (Fig. 1).

We quantified the persistence of infective virions under our standard conditions. The assay is represented schematically for one virus strain in Fig. 2. First, we produced "fresh" viruses by amplifying viruses in 10ml of $1x10^6$ algae/ml solution. The amplification was started with a modest number of virions (~$5x10^5$ virions/ml) and allowed to run for 24h on a shaker under the standard conditions. Solutions were then syringe-filtered through 0.45µm, and the virion concentration in the filtrates was immediately quantified by flow cytometry. We then prepared virion solutions with different concentrations for each strain: in deep well plates, we combined filtrates and BBM to produce 1.5ml solutions containing $5x10^4$, $5x10^3$, $5x10^2$, and $5x10^1$ virions/ml. The solutions were pipetted separately, so that they were statistically independent. The solutions were mixed and then aliquoted into five sets of culture plates, which were sealed with transparent foil and left under the standard conditions. After 0 days (i.e. on the same day as filtration), 7d, 14d, 21d, and 28d, we used a set of culture plates to measure the concentration of infective virions: 10µl from each solution was added to 16 culture wells containing 190µl of $1.05*10^6$ algae/ml solution (also in culture plates). These were kept on a shaker under the standard conditions for 4 days, after which we measured the OD_{680} to determine which culture wells contained viable algae (virus-negative) and which did not (virus-positive). Because one set of culture plates was prepared for every time point, the time points were statistically independent of each other.

The data we collected was the proportion of virus-positive wells over time; we used a generalized nonlinear regression model to extract our parameters of interest. The proportion of virus-positive wells follows a binomial distribution with 16 trials and a success probability of $P(virus^+\ well)$. The latter is calculated using the Poisson distribution:

$$P(virus^+\ well) = P_{Poisson}(\geq 1\ infective\ virion\ in\ the\ well) \quad \text{(Eq. 6.1)}$$

$$P(virus^+\ well) = 1 - P_{Poisson}(0\ infective\ virions\ in\ the\ well) \quad \text{(Eq.6.2)}$$

$$P(virus^+\ well) = 1 - e^{-expected\ number\ of\ infective\ virions} \quad \text{(Eq. 6.3).}$$

The expected number of infective virions depends on the number of virions added to each culture well V_{init} (10µl of $5*10^4$, $5*10^3$, $5*10^2$, and $5*10^1$ virions/ml solutions, i.e. 500, 50, 5, or 0.5 virions), the frequency of infective virions when the solution is fresh s, and the decay rate over time. At first, we fit a simple exponential decay model,

$$P(virus^+\ well) = 1 - e^{-s*V_{init}*e^{-m*t}} \quad \text{(Eq. 7),}$$

based on previous work for aquatic viruses (e.g. Cottrell & Suttle, 1995; Noble & Fuhrman, 1997; Demory *et al.*, 2021b). Here the decay term is e^{-m*t}, where m is the constant rate of decay, and t is the time in days. This simple model was a poor fit for many of the virus strains, however. Upon

investigation, these strains had higher decay rates at the beginning of the experiment than at the end. Therefore, we also fit a model with one additional parameter:

$$P(virus^{+}\ well) = 1 - e^{-(s*r*V_{init}+s*(1-r)*V_{init}*e^{-m*t})} \quad \text{(Eq. 8).}$$

This is a biphasic model, where the 'expected number of infective virions' term is split into two parts: $s * r * V_{init}$ represents a subpopulation of robust infective virions, which does not decay over time; $s * (1 - r) * V_{init} * e^{-m*t}$ represents a subpopulation of fragile infective virions, which decays exponentially. The probability that a fresh infective virion is robust is r. We chose to fit this model because it is the simplest possible extension of Eq. 7, and because it fit our data very well. We don't exclude that other possibilities, e.g. a model where the robust fraction decays at a slower rate, could also fit the data well. We fit Eq. 7 and Eq. 8 to our data using generalized nonlinear regression models (in R version 3.6.1, R Core Team, 2014; function "gnlr" in package "gnlm", Swihart & Lindsey, 2019) with binomial response variables. The parameters s, r, and m were inverse logit-transformed to keep them in the interval [0,1] (m can technically be larger than 1, but in practice the decay rates were much lower). Parametric bootstrapping was used to obtain 95% CIs for each parameter. The models were run separately for each viral strain, and we used the Akaike Information Criterion (AIC, Akaike, 1974) to compare the fit of the two models. A ΔAIC < -2 is strong support for the biphasic model. The model fit was assessed by visually judging the fit and distribution of residuals for the biphasic model (Eq. 8, Supp. Fig. 2).

Biphasic decay was confirmed in a separate experiment, as was the consistency of the fits for s, r, and m (Lievens *in prep*).

Comparison of mOSG and mP assays

By comparing the results of the mOSG and mP assays, we can derive the final traits in the life cycle: the probability that a depolarized cell completes the life cycle (c) and the burst size per completed cell (b_c) (Fig. 1). We define "completion" as lysis with release of virions.

Because infectivity is a compound trait, made up of successful depolarization and completion of the life cycle, the completion probability c can be derived from s and d (see Fig. 1):

$$c = s/d \quad \text{(Eq. 9).}$$

Comparisons between two experiments should be approached with caution. One point of difference is that the filtrates used for the mOSG assay were stored at 4°C for 2-8 days before the assay, and the mP assay filtrates were not. However, previous experiments show that s is unaffected by 4°C storage for at least 9 days (J. Clot & E.J.P. Lievens, unpublished data for strain PBCV-1), so this difference is unlikely to affect our calculations. A second difference is that the algae were centrifuged before the mOSG experiment to concentrate them. It is possible that this affected their susceptibility to depolarization (i.e. d) or stability when infected (i.e. c). In this case, we would expect the strains in each virus group to be affected equally. Finally, due to Covid-19 restrictions there was a 3-month delay between the two experiments, and we had to use separate batches of the host algae. The algae batches were grown from the same agar slants, however, so at most we could expect an environmental effect on s that affected all strains within a group.

We can then derive the average burst size per completed cell b_c as

$$b_c = b_d/c \quad \text{(Eq. 10),}$$

because the burst size of depolarized cells that don't complete the life cycle is 0 (see Fig. 1).

The bootstraps from the mOSG and mP assays were used to calculate confidence intervals for c and b_c. For example, each of the 999 bootstrapped values of s was divided by the corresponding bootstrapped value of d, and the resulting 999 outputs were used to calculate the 95% CI for c.

Growth assay

Finally, we added a test of relative growth to the mP assay (not shown in Fig. 2), using the "fresh" filtrates prepared at the start of that assay. For each viral strain, fresh filtrate was combined with the appropriate alga in a culture plate (2 wells per strain), to a final volume of 0.2ml containing $1*10^6$ algae/ml and 2500 or 25000 virions/ml. The plate was put on a shaker under the standard conditions for 24h, and then centrifuged for 15min at 2000g to separate algae and viruses. The virion concentration of the supernatants was measured by flow cytometry; we used the relative increase in virions/ml as a measure of viral growth rate.

Statistical analysis of the trait results

Our statistical analyses explored the diversity of the traits and looked for potential trade-offs. All analyses were done in R version 3.6.1 (R Core Team, 2014) and used only the retained trait estimates (see Results).

To examine the trait diversity within and among virus groups, we fit ANOVAs to each trait measured in the mOSG and mP assays. First, we used standard ANOVAs to partition variance among the virus groups (NC64A viruses, SAG viruses, Osy viruses). These used the full dataset, but could not account for the phylogenetic dependence between the strains. Second, we used phylogenetic ANOVAs to test for virus group effects. These analyses accounted for phylogenetic dependence (Garland *et al.*, 1993), but were restricted to the strains with a known phylogenetic position (n = 14 NC64A viruses, 1 Osy virus, 6 SAG viruses; Table 2). Finally, we used phylogenetic ANOVAs to partition variance among the virus clades. This accounted for the paraphyletic nature of the NC64A viruses, which are divided into a PBCV-1 clade and an NY-2A clade by the Osy strain OSyNE-5 (Quispe *et al.*, 2017; Rodrigues *et al.*, 2022). For each series of ANOVAs, we corrected for multiple testing with Holm's method (Holm, 1979). Trait k was transformed by $*10^9$ for computational reasons, and traits b_d, r, and b_c were *ln*-transformed. ANOVAs were run using the 'aov' function in base R and the 'phylANOVA' function in the 'phytools' package (Revell, 2012).

We also used correlational analyses to look for signals of trade-offs between the traits. We focused on the NC64A viruses, as they were all tested on the same algal strain. First, we looked for associations between the independent life history traits (traits marked in blue in Fig. 1). We tested for pairwise correlations using Spearman's rank correlations, weighted for the precision of each estimate by 1/√(product of the CI breadth of trait 1 and trait 2). We combined functions 'wrank' from the 'wCorr' package and 'wtd.cor' from the 'weights' package to produce these correlations (Pasek, 2021). They were then corrected for multiple testing using Holm's method (Holm, 1979). Trait k was transformed by $*10^8$ for computational reasons, and trait b_c was *ln*-transformed. We also applied a Principal Component Analysis (PCA) to the independent traits. To deal with the missing values in our dataset, we used the 'Ipca' and 'PairCor' methods described in Dray & Josse (2015). Ipca uses an iterative algorithm to impute missing values, while PairCor uses a pairwise correlation approach to avoid missing values. We used Podani et al.'s (2021) PairCor code, and the biplot extension proposed in the same paper. For Ipca, we used the function 'imputePCA' from the 'missMDA' package (Josse & Husson, 2016). If the two missing value methods produced inconsistent results, we considered that the PCA was not robust. Trait k was transformed by $*10^8$, and trait b_c was *ln*-transformed. Second, we tested for specific constraints that have been found or suggested in the literature (listed in Table 3). As above, we used weighted Spearman's rank correlations and corrected for multiple testing using Holm's method. The relative growth and multiplication rate were *ln*-transformed.

As trade-offs can be masked by quality effects in correlational analyses (Stearns, 1989), we repeated the analyses in the previous paragraph with the 'highest quality' NC64A viruses. Our proxy for quality was the relative growth of the viruses in the growth assay. The only difference was in the transformations for the PCA: trait b_c was not *ln*-transformed, and trait *r* was logit-transformed.

Results

The trait estimates and their 95% CIs are shown in the upper panels of Fig. 3. In a few cases, the mOSG or mP assays failed or were incomplete. For the mOSGC assay, one strain was not used due to insufficient virion concentration in the filtrate (OSyNE-5B-M2), four strains did not grow within the sampling time (AR158[1], NY-2A, Canal-1, NES-4A-S1), and several others had incomplete growth (AR158[2], MA-1D, OSyNE-4B-M2, OSyNE-4B-S2, OSyNE-5, OSyNE-5B-S1). For the mP assay, three strains did not produce any virus-positive wells (AR158[1], Canal-1, NES-4A-S1), and one strain had an incomplete assay with no decay (NY-2A). We regarded the parameters fit to incomplete growth or decay data as inherently flawed, and excluded these estimates and their derivatives from all further analyses (orange in Fig. 3). The statistical model was a poor fit in one case (MO0605SPH for *d* and b_d); these estimates and their derivatives were also excluded (red in Fig. 3). Finally, we excluded trait estimates with unreasonably large CIs from all further analyses (red in Fig. 3). The retained estimates and CIs are listed in Supp. Table 1.

16 out of the 31 strains that completed the mP assay had strong support for the biphasic viral persistence model (Eq. 8; strong support when $\Delta AIC < -2$, Supp. Table 1); the remaining 15 strains had equivocal support for the exponential and biphasic models ($2 < \Delta AIC < -2$). Fig. 3 presents the results of the biphasic models.

Trait diversity within- and among chlorovirus groups

The virus traits were remarkably diverse. There was a 5- to 75-fold variation in retained estimates for every trait, and the trait ranges often overlapped between chlorovirus groups (Fig. 3, lower panels). To investigate this further, we partitioned the trait variance within- and among groups using ANOVAs.

First, we used a standard ANOVA to partition variance among the virus groups (NC64A viruses, SAG viruses, and Osy viruses). Group explained a significant proportion of the variance for the adsorption constant *k*, the mean latent period μ_l, the SD of latent period σ_l, and the burst size per depolarized cell b_d (proportions respectively 0.33, 0.86, 0.68, 0.56; *p* respectively 0.01, < 0.0001, < 0.0001, 0.01 after correction for multiple testing; Supp. Table 2).

The per-group phylogenetic ANOVA yielded similar variance partitioning results (Supp. Table 2). None of the group effects were statistically significant, reflecting the strong phylogenetic dependence in the dataset.

We also used a phylogenetic ANOVA to partition the variance among the virus clades (PBCV-1 clade, NY-2A clade, SAG viruses, and OSy viruses). The results were very similarly to the per-group phylogenetic ANOVA, with two notable exceptions (Supp. Table 2): clade explained four times more of the variance in specific infectivity *s* (0.45 vs. 0.11 per group) and twelve times more of the variance in decay rate *m* (0.37 vs. 0.03). These effects were due to the higher *s* and *m* values in the PBCV-1 clade compared to the NY-2A clade. Clade also explained more of the variance in burst size per completed cell b_c (0.11 vs. 0.001), but this difference is unreliable due to the many missing values in the NY-2A clade. Again, none of the clade effects were statistically significant.

Correlations between traits in the NC64A viruses

Correlations between life cycle traits can suggest the existence of constraints or life history strategies. We used our largest virus group, the NC64A viruses, to look for such associations.

First, we analyzed the associations among independent traits (traits marked in blue in Fig. 1). Only three pairwise correlations were statistically significant after correction for multiple testing (Fig. 4A, Supp. Table 3): the burst size per completed cell b_c and depolarization probability d were negatively correlated with the completion probability c (resp. ρ = -0.86 and -0.8, p = 0.007 and 0.01) and positively correlated with each other (ρ = 0.86, p = 0.003). When this dataset was used for PCA, the PairCor and Ipca methods were inconsistent (data not shown), so these PCA results are not interpreted further.

Second, we looked for additional correlations which we specifically hypothesized might occur (Fig. 4B, Supp. Table 3). Short-term virion quality (represented by the specific infectivity s) was significantly correlated with long-term virion quality in the form of decay rate m (ρ = 0.83, p = 0.0004), but not in the form of the robust fraction r. Survival (represented by the decay rate m) was significantly correlated with reproduction in the form of relative growth (ρ = 0.76, p = 0.003), but not with the 'multiplication rate' as in De Paepe & Taddei (2006). Finally, offspring quantity (burst size per infected cell b_d) and quality (represented by the specific infectivity s) were not significantly correlated.

Correlations between traits in the fastest-growing NC64A viruses

Because overall quality can confound the detection of constraints (Stearns, 1989), we repeated the analyses from the previous section on the 12 fastest-growing NC64A viruses. These were: AN69C, CA-4A, CV-K1, CvsA1, IL-3A, IL-5-2s1, MA-1E, NE-JV-4, NYs-1, PBCV-1, WNE-10B-L2, XZ-4A (see Fig. 4C, Supp. Table 1).

For most pairwise comparisons of independent traits, the correlation coefficients were similar for the restricted and full datasets (Fig. 5A, Supp. Table 3). Notable exceptions were the correlations between decay rate m and adsorption constant k and robust fraction f, which changed from positive to negative; and the loss of the negative correlation between completion probability c and genome size. However, only the positive correlation between the burst size per completed cell b_c and the depolarization probability d was significant in the restricted dataset (ρ = 0.85, p = 0.04 after correction for multiple testing; Supp. Table 3), likely due to the smaller sample size. PCA of the independent trait data was robust to the missing-value method. It supported the association between burst size per completed cell b_c, depolarization probability d, and completion probability c, and associated this axis with the adsorption constant k (Fig. 5B). The mean and SD of latent period μ_l and σ_l were positively associated, and decay rate m was negatively associated with the robust fraction r.

Two of the additional correlations that were strongly positive when tested in all NC64A viruses were very different in the subset of fastest-growing strains: the (non-significant) correlation between specific infectivity s and the robust fraction r became negative, and the correlation between relative growth and decay rate m disappeared (Fig. 5C). None of the additional correlations were significant after correction for multiple testing (Supp. Table 3).

Discussion

Viral life histories shape their epidemiology, ecosystem effects, and evolutionary potential. In this study, we modified classic methods to quantify the life cycle traits of 35 chloroviruses from the NC64A, Osy, and SAG virus groups. We found high trait diversity among these viruses, with evidence

for trade-offs between some traits. We discuss these findings below, and also highlight new insights into the chlorovirus life cycle.

The traits we have measured include genome, virion, and virocell performance traits (DeLong *et al.*, 2022) – we focus on their performance aspects here. The virion and virocell phenotypes were probably mediated by interactions between the viral genotype, the host genotype, and the environment (G_V x G_H x E interactions), which should be kept in mind when comparing traits between groups and with other studies.

High trait diversity within and across chlorovirus groups

The first goal of our study was to explore the trait diversity of the chloroviruses, which influences their evolvability and the range of their ecological effects. The strains we used were known to vary in genome size, production of extracellular matrix, and plaque size (Supp. Table 1). We can now add that they vary substantially in every life cycle trait, both within and between virus groups (Fig. 3).

We can assume that the within-group diversity in virus traits is a consequence of genetic variation, as the strains were tested in the same host and environment (G_H and E kept constant). This genetic association would allow an evolutionary response to occur if selection favors a particular phenotype[4], which may happen during the progression of an epidemic (Frank, 1996; Bolker *et al.*, 2010; Berngruber *et al.*, 2013), as host densities change (Abedon *et al.*, 2003; Heineman & Bull, 2007), or in response to abiotic changes (Alizon *et al.*, 2009; Dessau *et al.*, 2012; Heineman & Brown, 2012). The occurrence of viral evolution in nature is supported by work on NC64A, Osy, and SAG viruses in natural ponds (Quispe *et al.*, 2016), which showed that the frequencies of plaque size phenotypes varied over the course of a year. In future, combining trait data with genomic data (Jeanniard *et al.*, 2013; e.g. Rodrigues *et al.*, 2022) could allow the creation of a genotype-to-phenotype map to explore chlorovirus evolution (DeLong *et al.*, 2022).

Attributing the between-group variation to genetic differences is more difficult, as the viruses could not be tested on a common host (only E kept constant). It is intriguing, however, that the SAG viruses had shorter latent periods and slower adsorption. The SAG viruses infect *C. heliozoae*, which forms symbioses with the heliozoan *Acanthocystis turfacea*, while the NC64A and Osy viruses infect *C. variabilis*, which symbioses with the ciliate *Paramecium bursaria* (Van Etten *et al.*, 2020). Predation of the ciliate host is known to affect Osy-NE-ZA1 growth (DeLong *et al.*, 2016, 2018; Al-Ameeli *et al.*, 2021), so it is possible that virus traits respond to the broader ecological context of the heliozoan or ciliate hosts.

The natural phenotypic diversity is likely to be even higher than the 5- to 75-fold range we measured. Previous work has shown that the expression of chlorovirus traits depends on the host genotype (G_H effects)(Quispe *et al.*, 2017) and on environmental (E) effects such as light conditions (Van Etten *et al.*, 1983, I. Agarkova unpublished data), temperature (Horas *et al.*, 2018, I. Agarkova unpublished data), nutrient ratios (Clasen & Elser, 2007; Cheng *et al.*, 2015), and the host's growth phase (Van Etten *et al.*, 1983, E.J.P. Lievens unpublished data). It is likely that these effects interact with virus strain (G_V x G_H and G_V x E effects) and with each other (G_H x E and G_V x G_H x E effects), further enriching the overall phenotypic diversity. Interestingly, the relative lysis times we found

[4] Here we assume that the group level corresponds to the species level, within which evolution can occur. The chlorovirus groups infect the same hosts and a high protein sequence similarity (≥ 92.6%, Jeanniard *et al.*, 2013; see also Rodrigues *et al.*, 2022), supporting this approach. Yet considering the paraphyletic nature of the NC64A viruses (Quispe *et al.*, 2017; Rodrigues *et al.*, 2022), it may be more accurate to use virus clade as a species proxy. This would not affect our conclusion, as we also found ample within-clade phenotypic variation.

corresponded well to previous studies of multiple chloroviruses, but the relative burst sizes did not (Supp. Table 1, Van Etten *et al.*, 1988; Schiano di Visconte *et al.*, 2022). This suggests that different traits have different G_V x E effects, as found in other host-parasite systems (Hall *et al.*, 2017). Future research could examine the extent, and ideally the functional basis, of this (lack of) plasticity.

Evidence for constraints and life history strategies in the NC64A viruses

We used our largest virus group, the NC64A viruses, to look for trait correlations that could suggest the existence of trade-offs among life cycle traits. Correlations cannot prove that a functional constraint exists (Zera & Harshman, 2001; Agrawal *et al.*, 2010), and conversely quality effects can prevent trade-offs from manifesting as correlations (Stearns, 1989) (and indeed many of the correlation coefficients reversed or approached 0 in the fastest-growing NC64A viruses, Fig. 5A&C). Nonetheless, correlational analyses are an important explorative step, and allow comparisons with the existing literature.

Among the independent life cycle traits, we found that virus strains with higher depolarization probabilities (d) also had higher burst sizes per completed cell (b_c) and lower completion probabilities (c). This correlation was visible for all NC64A viruses and for the high-quality subset (Fig. 4A, non-significant in Fig. 5A). The negative correlation between d and c arises because the specific infectivity s is essentially constant when compared to the high variation in d, and $c = s/d$ (Supp. Fig. 3). Dividing b_d by c reranks a few crucial strains to produce the negative correlation between b_c and c (Supp. Fig. 3) and strengthen the positive association with d. The precise correlations should be treated with some skepticism, considering the breadth of the confidence intervals around c (Fig. 3). However, the overall pattern does suggest an area of 'biological impossibility', which is supported by the SAG viruses (Supp. Fig. 3). If this is a trade-off, it is unclear why depolarization probability and progeny number should come at the cost of completion probability. Perhaps the production of many depolarizing-capable virions is more error-prone, or over-exploits host resources. The association with the adsorption constant k in the fastest-growing NC64A viruses (Fig. 5B) could fit either context, assuming that well-adsorbing virions are more complicated or more resource-intensive to produce.

There were no other significant correlations between the independent traits. In particular, there was no relationship between the mean latent period μ_l and burst size per completed cell b_c, which has been suggested as a generalizable trade-off for lytic viruses (Goldhill & Turner, 2014). Replacing b_c with the infective burst size ($s*b_c$) or nucleotide production per completed cell (genome size*b_c) did not produce correlations with μ_l either (data not shown). The one-dimensional trade-off between lysis time and burst size may be obscured by the comparative nature of the analysis, or it may not exist for the NC64A viruses.

A striking pattern emerged from the additional correlation tests: viruses with lower decay rate m also had lower specific infectivity s (Fig. 4B[5], non-significant in Fig. 5C). In other words, some virus strains produced a high frequency of initially infective virions that decayed quickly, while others produced a low frequency of infective virions that decayed slowly. In the full dataset, viruses with slower decay also had lower relative growth (Table 3, Fig. 4B). This correlation was driven by the

[5] The four slowest-growing strains are immediately obvious in Fig. 4B. Considering the extremely low growth rates of these strains (Supp. Table 1), it is possible that mP assay wells inoculated with small numbers of infective virions did not have time to become clear. This would have led to an underestimate of s. However, even a 10-fold increase in s would not have changed the ranking of the strains, i.e. would not have affected the Spearman correlation coefficients. Furthermore, the positive (though non-significant) correlation between s and m in the subset of fastest-growing strains cannot be affected by this potential bias.

slowest-growing strains (AR158, MA-1D, NY-2A, NY-2B, Supp. Table 1), which all belonged to the NY-2A clade. (The NY-2A clade also contains fast-growing strains, which is why the per-clade ANOVA explained more variance in *s* and *m* but not the majority of it.) One interpretation of these results is that NC64A viruses can follow a short-term or long-term life history strategy, and that the long-term strategy evolved to an extreme in the NY-2A clade at the cost of (short-term) relative growth. However, observations under more natural conditions would be necessary to support this hypothesis. Indeed, the very slow growth in the NY-2A clade could simply indicate that these strains are best adapted to another host genotype, whose ecology favors very slow decay.

Finally, we found a correlation between survival (low decay rate *m*) and reproduction (high relative growth, Fig. 4B), as in previous studies with phages (correlations: De Paepe & Taddei, 2006; Dessau *et al.*, 2012; confirmed trade-offs: Heineman & Brown, 2012; García-Villada & Drake, 2013). Interestingly, we did not find a correlation when reproduction was calculated as the multiplication rate following the classic example in De Paepe & Taddei (2006) (Fig. 4B). The multiplication rate is designed to predict relative growth; that it does not do so here suggests there is a missing trait that plays a crucial role in chlorovirus growth.

New insights into chlorovirus life cycles: failure to depolarize vs. failure to complete

Overall, the chlorovirus virions had a high failure rate: depending on the strain, only 0.4 to 24% of freshly-produced virions were infective (specific infectivity, Fig. 3). Our estimates were lower than those found previously, e.g. 10% compared to 25-30% for PBCV-1 (Van Etten *et al.*, 1983), a difference that may be due to the lower quality of the medium (E effects, Bratbak *et al.*, 1998; Maat & Brussaard, 2016; Bachy *et al.*, 2018) (cf. Tseng & Myers, 2014) or to a difference in sensitivity of liquid culture vs. plaque assays. Defective virions are a well-known aspect of virus biology (Klasse, 2015), and in PBCV-1 they include empty capsids and capsids with different membrane conformations (Agarkova *et al.*, 2014). Here we separated viral failure into performance traits: an inability to depolarize the host cell and an inability to complete the life cycle.

The depolarization probability varied widely between strains (Fig. 3). The 'depolarization' step in our model actually includes three events: first, the host cell wall is digested by a conserved virion protein, A561L (Agarkova *et al.*, 2021); next, the viral and host membranes fuse, most likely due to turgor pressure in the host cell (Thiel *et al.*, 2010); finally, virion-associated K^+ channel proteins depolarize the cell (Frohns *et al.*, 2006; Thiel *et al.*, 2010). The ability to successfully depolarize a host is therefore dependent on specific, pre-packaged virion proteins (it is a virion trait, DeLong *et al.*, 2022). We hypothesize that the interstrain variation in depolarization probability is caused by variation in the efficiency or copy number of the A561L or K^+ channel proteins (K+ channel variation in Frohns *et al.*, 2006; A561L: PBCV-1 has ~60 copies per virion, Dunigan *et al.*, 2012). Transcriptomic or proteomic studies on multiple virus strains should shed light on the underlying mechanism.

Surprisingly, we find that an inability to complete the life cycle is the biggest hurdle for chloroviruses: in all but one strain, fewer than half of the depolarized host cells produced progeny virions (completion probability 0.01-0.42, Fig. 3). These low values may have been affected by our assumption that all virions were capable of adsorbing. If there was a "residual fraction" of non- or slow-adsorbing virions (Gallet *et al.*, 2012), the specific infectivity would actually be $s = P(\text{capable of adsorbing})*d*c$, and we would have underestimated c (and overestimated b_c). Yet even if half of the virions were incapable of adsorbing, the corrected completion probability would fall below 50% for most strains. Completion probability is a virocell trait (DeLong *et al.*, 2022) that depends on both host and virus. The high failure rates might reflect errors in the viral capsid construction (possibly at play in Agarkova *et al.*, 2014), suboptimal physiological states in the host (cf. Clasen & Elser, 2007;

Cheng *et al.*, 2015), or evolutionarily mismatched host-virus combinations (possibly at play in Quispe *et al.*, 2017). Viral failure could also be due to active host interference. *Chlorella variabilis* has many homologs of genes that respond to viral infection in higher plants, including RNA silencing genes (Rowe *et al.*, 2013). If a virus-repression mechanism protected the surrounding kin cells, it could be viable even if the focal cell dies (Refardt *et al.*, 2013). Finally, increasing the completion probability could come at the cost of some other virus trait (Goldhill & Turner, 2014). As discussed above, the cost could be in depolarization quality or progeny number; if not, this does not invalidate the possibility of a trade-off constraining completion probability.

New insights into chlorovirus life cycles: biphasic persistence

We discovered that many chloroviruses have biphasic or "tailing" persistence, with 0-10% of the initial infective virions being resistant to decay in our model (robust fraction *r*, Fig. 1 & 3). In reality these virions almost certainly would decay, but this was not detected in our experiment. Biphasic decay is found in many virus species, and can be caused by several factors. 1) Changes in medium properties through time (Hiatt, 1964). In this case we would have expected the same biphasic pattern to occur across all strains, so this is not likely. 2) Adhesion to organic particles (Agarkova *et al.*, 2014; Pinon & Vialette, 2018). In this case, we would expect to see a larger robust fraction in the fast-growing strains, because they caused more lysis, and thus produced more organic matter, in the first step of the mP assay. We do not see this pattern (e.g. *r* between 0.1 and 5% for the fast-growing NC64A viruses, Fig. 3). 3) Viral aggregation (Pinon & Vialette, 2018). Chloroviruses are likely to aggregate, and different strains could vary in their tendency to do so. 4) Two concurrent decay processes causing differing degrees of damage (Koch, 1960; Hiatt, 1964; Roy *et al.*, 1982; cf. Beck *et al.*, 2014). If the first process (e.g. damage to the capsid) occurs rapidly but leaves some probability of successful infection, and the second process (e.g. DNA denaturation) occurs slowly and leads to complete inactivation, biphasic kinetics emerge. The variation between strains could be due to variation in the stability of the two targets of inactivation; the strains where $r = 0$ would then lack one target or have both decay at the same rate. 5) The presence of a more resistant subpopulation with slower decay. These might be virions with fewer production errors (Beauchemin *et al.*, 2019), or virions with a specifically different phenotype (Hiatt, 1964; Brouwer *et al.*, 2017).

For possibilities 3-5, we could expect selection to optimize the biphasic pattern in response to each strain's native environment. Selection could act synergistically on the decay rate *m* and robust fraction *r* to produce high vs. low-persistence types. There is indeed a synergistic association between *m* and *r* in the fast-growing NC64A viruses (Fig. 5B), though not across the board (Fig. 4B). Alternatively, the robust fraction could reflect an adaptation to uncertainty in the environment. If long-term infectivity comes at a cost of short-term success, then producing two virion types could allow chloroviruses to profit from patches of concentrated algae (Frank, 1996; Berngruber *et al.*, 2013) and to survive their seasonal environments (Long & Short, 2016). In this case, biphasic persistence could be a bet-hedging strategy (constant *r*) or a plastic strategy (*r* varying in response to environmental cues); both types have been demonstrated for various virus traits (bet-hedging: Gallet *et al.*, 2012; Chaturvedi *et al.*, 2020)(plasticity: Leggett *et al.*, 2013; Erez *et al.*, 2017; Bruce *et al.*, 2021). Again, there is a trend in this direction in the fast-growing NC64A viruses (negative association between specific infectivity *s* and *r*, Fig. 5B), but not across the board (Fig. 4B).

It is striking that we find biphasic decay in all the chlorovirus groups, because the existing work on phytoplankton viruses typically assumes exponential decay (i.e. decay at a constant rate) (Suttle & Chan, 1994; Cottrell & Suttle, 1995; Garza & Suttle, 1998; Šulčius *et al.*, 2015; Long & Short, 2016; Demory *et al.*, 2017, 2021a; b). This may be influenced by practical limitations on the duration of experiments or by simplifying assumptions from other literatures (Pinon & Vialette, 2018). Though

assuming exponential decay may be appropriate in many cases, it seems unlikely that the chloroviruses are the only algal viruses with a robust fraction (possible non-linearity in Tomaru *et al.*, 2005). Finding biphasic decay in other phytoplankton viruses could resolve some outstanding questions about their ecology, such as their ability to form 'seed banks' that persist outside blooms (Long & Short, 2016). It would also affect our understanding of aquatic microbial communities and nutrient cycling, in which viral infection and decay play important roles (Mojica & Brussaard, 2014).

Applicability of the methods and future work

We hope that these methods will be useful to other virologists interested in life history traits. By leveraging the distinction between MOP and MOI, the mOSG and mP assays measure more traits than assays based on one or the other (e.g. Van Etten *et al.*, 1983; Tomaru *et al.*, 2005; Taylor *et al.*, 2018). The high-throughput flow cytometry also makes them more efficient than e.g. quantification through plaque assays. The assays should be applicable to any culturable lytic virus that can be counted on a flow cytometer, which now includes many aquatic (Brussaard, 2004) and human viruses (Lippé, 2018). The statistical models can be edited to reflect life cycle differences. For example, our models assume that burst size is constant because multiple infections are impossible (see below, Greiner *et al.*, 2009). This is equivalent to a system where multiple infections are possible, but do not affect burst size. If multiple infections are possible and do affect burst size, the equations could be extended to include a facilitation or competition factor. Finally, in systems where no information is available, some inferences can be made from the relative amplitudes of the mOSG curves. These should be related to MOP via a Poisson probability function if burst size is independent of MOP (Supp. Fig. 4).

Further work on the chlorovirus life cycles could support or refute some aspects of our models. As discussed above, we assumed there was no "residual fraction" during adsorption, and that robust infective virions never decay (Fig. 1). These are probably unrealistic assumptions, which could be tested by longer studies of adsorption or persistence. We also assumed that all parameters were independent of MOP, meaning that each infection was started by a single virion (Greiner *et al.*, 2009) and was unaffected by other virions attaching to or digesting the cell wall of the host. Our data is consistent with this assumption, but it has limited power to detect deviations (Supp. Fig. 4). A previous study found an effect of MOI on burst size in PBCV-1 (Van Etten *et al.*, 1983), and 'lysis from without' and dual infection have been observed for chloroviruses at very high MOIs (J.L. Van Etten, unpublished data; Graves *et al.*, 2001). Future work at higher MOPs or with different chloroviruses may need to incorporate MOP-dependencies (cf. Brown & Bidle, 2014; Taylor *et al.*, 2018). Finally, our methods estimated an average burst size, while studies in other viruses have shown that per-cell burst size can vary by orders of magnitude (Kannoly *et al.*, n.d.; Delbrück, 1945; Timm & Yin, 2012). Observing the intercellular variation in burst size in chloroviruses could clarify the nature of infection completion: low variation would indicate pass/fail infections, while a very high variation would suggest quantitative barriers to completion (Hall *et al.*, 2017).

Conclusion

A proper understanding of the ecological impact and evolutionary potential of viruses rests on a knowledge of their life cycle traits. We showed that the chloroviruses have high phenotypic diversity across their entire life history, both within and across host range groups. This suggests that they are evolutionarily flexible, although they may be constrained by e.g. a survival-reproduction trade-off or depolarization-completion trade-off. The chloroviruses also had strong variation in relative growth, decay rate, and long-term persistence capabilities, which are likely to have strong effects on their

ecology. These results confirm the importance of studying viral life cycle traits, and will hopefully prompt similar research into other phytoplankton viruses.

Acknowledgements

E.J.P.L. thanks J. Pantel for feedback on the statistical modelling, J. Clot for help with the viruses, and R. Hermann for transferring algae during lockdown. We acknowledge the flow cytometry centre (FlowKon) at the University of Konstanz for the use of flow cytometers and the expert support in instrument usage and data analysis.

References

Abedon, S.T., Hyman, P. & Thomas, C. 2003. Experimental Examination of Bacteriophage Latent-Period Evolution as a Response to Bacterial Availability. *Appl. Environ. Microbiol.* **69**: 7499–7506. doi:10.1128/AEM.69.12.7499-7506.2003

Adams, M.H. & Wassermann, F.E. 1956. Frequency Distribution of Phage Release in the One-Step Growth Experiment. *Virology* **2**: 96–108.

Agarkova, I., Hertel, B., Zhang, X., Lane, L., Tchourbanov, A., Dunigan, D.D., *et al.* 2014. Dynamic attachment of Chlorovirus PBCV-1 to Chlorella variabilis. *Virology* **466-467**: 95–102. doi:10.1016/j.virol.2014.07.002

Agarkova, I. V., Lane, L.C., Dunigan, D.D., Quispe, C.F., Duncan, G.A., Milrot, E., *et al.* 2021. Identification of a chlorovirus pbcv-1 protein involved in degrading the host cell wall during virus infection. *Viruses* **13**: 1–19. doi:10.3390/v13050782

Agrawal, A.A., Conner, J.K. & Rasmann, S. 2010. Tradeoffs and Negative Correlations in Evolutionary Ecology. In: *Evolution After Darwin: the First 150 Years* (M. A. Bell, W. F. Eanes, D. J. Futuyma, & J. S. Levinton, eds), pp. 243–268. Sinauer Associates

Akaike, H. 1974. A new look at the statistical model identification. *IEEE Trans. Automat. Contr.* **19**: 716–723. doi:10.1109/TAC.1974.1100705

Al-Ameeli, Z.T., Al-Sammak, M.A., DeLong, J.P., Thomas, S., Dunigan, D.D. & Van Etten, J.L. 2021. Catalysis of chlorovirus production by the foraging of Bursaria truncatella on Paramecia bursaria containing endosymbiotic algae. *Microb. Ecol.* **9**: 2170.

Alizon, S., Hurford, A., Mideo, N. & Van Baalen, M. 2009. Virulence evolution and the trade-off hypothesis: history, current state of affairs and the future. *J. Evol. Biol.* **22**: 245–59. doi:10.1111/j.1420-9101.2008.01658.x

Bachy, C., Charlesworth, C.J., Chan, A.M., Finke, J.F., Wong, C.H., Wei, C.L., *et al.* 2018. Transcriptional responses of the marine green alga Micromonas pusilla and an infecting prasinovirus under different phosphate conditions. *Environ. Microbiol.* **20**: 2898–2912. doi:10.1111/1462-2920.14273

Baty, F., Ritz, C., Charles, S., Brutsche, M., Flandrois, J. & M, D.-M. 2015. A Toolbox for Nonlinear Regression in R: The Package nlstools. *J. Stat. Softw.* **66**: 1–21.

Baudoux, A.-C. & Brussaard, C.P.D. 2005. Characterization of different viruses infecting the marine harmful algal bloom species Phaeocystis globosa. *Virology* **341**: 80–90.

Beauchemin, C.A.A., Kim, Y.-I., Yu, Q., Ciaramella, G. & DeVincenzo, J.P. 2019. Uncovering critical properties of the human respiratory syncytial virus by combining in vitro assays and in silico analyses. *PLoS One* **14**: e0214708. doi:10.1371/journal.pone.0214708

Beck, S.E., Rodriguez, R.A., Linden, K.G., Hargy, T.M., Larason, T.C. & Wright, H.B. 2014. Wavelength dependent UV inactivation and DNA damage of adenovirus as measured by cell culture infectivity and long range quantitative PCR. *Environ. Sci. Technol.* **48**: 591–598. doi:10.1021/es403850b

Belshaw, R., Gardner, A., Rambaut, A. & Pybus, O.G. 2008. Pacing a small cage: mutation and RNA viruses. *Trends Ecol. Evol.* **23**: 188–193. doi:10.1016/j.tree.2007.11.010

Berngruber, T.W., Froissart, R., Choisy, M. & Gandon, S. 2013. Evolution of virulence in emerging epidemics. *PLOS Pathog.* **9**: e1003209.

Bolker, B.M., Nanda, A. & Shah, D. 2010. Transient virulence of emerging pathogens. *J. R. Soc. Interface* **7**: 811–822.

Bratbak, G., Jacobsen, A., Heldal, M., Nagasaki, K. & Thingstad, F. 1998. Virus production in Phaeocystis pouchetii and its relation to host cell growth and nutrition. *Aquat. Microb. Ecol.* **16**: 1–9. doi:10.3354/ame016001

Brouwer, A.F., Eisenberg, M.C., Remais, J. V., Collender, P.A., Meza, R. & Eisenberg, J.N.S. 2017. Modeling Biphasic Environmental Decay of Pathogens and Implications for Risk Analysis. *Environ. Sci. Technol.* **51**: 2186–2196. doi:10.1021/acs.est.6b04030

Brown, C.M. & Bidle, K.D. 2014. Attenuation of virus production at high multiplicities of infection in Aureococcus anophagefferens. *Virology* **466-467**: 71–81.

Bruce, J.B., Lion, S., Buckling, A., Westra, E.R. & Gandon, S. 2021. Regulation of prophage induction and lysogenization by phage communication systems. *Curr. Biol.* **31**: 5046–5051. doi:10.1016/j.cub.2021.08.073

Brussaard, C.P.D. 2004. Optimization of procedures for counting viruses by flow cytometry. *Appl. Environ. Microbiol.* **70**: 1506–1513.

Ceyssens, P.-J., Glonti, T., Kropinski, A.M., Lavigne, R., Chanishvilli, N., Kulakov, L., *et al.* 2011. Phenotypic and genotypic variations within a single bacteriophage species. *Virol. J.* **8**: 134.

Chaturvedi, S., Klein, J., Vardi, N., Bolovan-Fritts, C., Wolf, M., Du, K., *et al.* 2020. A molecular mechanism for probabilistic bet hedging and its role in viral latency. *Proc. Natl. Acad. Sci. U. S. A.* **117**: 17240–17248. doi:10.1073/pnas.1914430117

Cheng, Y.S., Labavitch, J. & VanderGheynst, J.S. 2015. Organic and Inorganic Nitrogen Impact Chlorella variabilis Productivity and Host Quality for Viral Production and Cell Lysis. *Appl. Biochem. Biotechnol.* **176**: 467–479. doi:10.1007/s12010-015-1588-0

Clasen, J.L. & Elser, J.J. 2007. The effect of host Chlorella NC64A carbon : phosphorus ratio on the production of Paramecium bursaria Chlorella Virus-1. *Freshw. Biol.* **52**: 112–122. doi:10.1111/j.1365-2427.2006.01677.x

Cottrell, M.T. & Suttle, C.A. 1995. Dynamics of a lytic virus infecting the photosynthetic marine picoflagellate Micromonas pusilla. *Limnol. Oceanogr.* **40**: 730–739.

De Paepe, M. & Taddei, F. 2006. Viruses' life history: towards a mechanistic basis of a trade-off between survival and reproduction among phages. *PLOS Biol.* **4**: e193. doi:10.1371/journal.pbio.0040193

Delbrück, M. 1945. The burst size distribution in the growth of bacterial viruses (bacteriophages). *J. Bacteriol.* **50**: 131–135.

DeLong, J.P., Al-Ameeli, Z., Duncan, G., Van Etten, J.L. & Dunigan, D.D. 2016. Predators catalyze an increase in chloroviruses by foraging on the symbiotic hosts of zoochlorellae. *Proc. Natl. Acad. Sci. U. S. A.* **113**: 13780–13784.

DeLong, J.P., Al-Ameeli, Z., Lyon, S., Van Etten, J.L. & Dunigan, D.D. 2018. Size-dependent catalysis of chlorovirus population growth by a messy feeding predator. *Microb. Ecol.* **75**: 847–853.

DeLong, J.P., Al-Sammak, M.A., Al-Ameeli, Z.T., Dunigan, D.D., Edwards, K.F., Fuhrmann, J.J., *et al.* 2022. Towards an integrative view of virus phenotypes. *Nat. Rev. Microbiol.* **20**: 83–94. doi:10.1038/s41579-021-00612-w

Demory, D., Arsenieff, L., Simon, N., Six, C., Rigaut-Jalabert, F., Marie, D., *et al.* 2017. Temperature is a key factor in Micromonas-virus interactions. *ISME J.* **11**: 601–612. doi:10.1038/ismej.2016.160

Demory, D., Liu, R., Chen, Y., Zhao, F., Coenen, A.R., Zeng, Q., *et al.* 2021a. Linking Light-Dependent Life History Traits with Population Dynamics for Prochlorococcus and Cyanophage. *mSystems* **5**: e00586–19.

Demory, D., Weitz, J.S., Baudoux, A.-C., Touzeau, S., Simon, N., Rabouille, S., *et al.* 2021b. A thermal trade-off between viral production and degradation drives virus-phytoplankton population dynamics. *Ecol. Lett.* **24**: 1133–1144. doi:10.1111/ele.13722

Dennehy, J.J. & Wang, I.-N. 2011. Factors influencing lysis time stochasticity in bacteriophage l. *BMC Microbiol.* **11**: 174.

Dessau, M., Goldhill, D., McBride, R.L., Turner, P.E. & Modis, Y. 2012. Selective Pressure Causes an RNA Virus to Trade Reproductive Fitness for Increased Structural and Thermal Stability of a Viral Enzyme. *PLoS Genet.* **8**. doi:10.1371/journal.pgen.1003102

Dray, S. & Josse, J. 2015. Principal component analysis with missing values: a comparative survey of methods. *Plant Ecol.* **216**: 657–667. doi:10.1007/s11258-014-0406-z

Dunigan, D.D., Cerny, R.L., Bauman, A.T., Roach, J.C., Lane, L.C., Agarkova, I. V., *et al.* 2012. Paramecium bursaria Chlorella Virus 1 Proteome Reveals Novel Architectural and Regulatory Features of a Giant Virus. *J. Virol.* **86**: 8821–8834. doi:10.1128/jvi.00907-12

Edwards, K.F. & Steward, G.F. 2018. Host Traits Drive Viral Life Histories across Phytoplankton Viruses. *Am. Nat.* **191**: 566–581.

Erez, Z., Steinberger-Levy, I., Shamir, M., Doron, S., Stokar-Avihail, A., Peleg, Y., *et al.* 2017. Communication between viruses guides lysis-lysogeny decisions. *Nature* **541**: 488–493. doi:10.1038/nature21049

Frank, S.A. 1996. Models of parasite virulence. *Q. Rev. Biol.* **71**: 37–78.

Frickel, J., Sieber, M. & Becks, L. 2016. Eco-evolutionary dynamics in a co-evolving host-virus system. *Ecol. Lett.* **19**: 450–459.

Frohns, F., Käsmann, A., Kramer, D., Schäfer, B., Mehmel, M., Kang, M., *et al.* 2006. Potassium Ion Channels of Chlorella Viruses Cause Rapid Depolarization of Host Cells during Infection. *J. Virol.* **80**: 2437–2444. doi:10.1128/jvi.80.5.2437-2444.2006

Furió, V., Moya, A. & Sanjuán, R. 2005. The cost of replication fidelity in an RNA virus. *Proc. Natl. Acad. Sci. U. S. A.* **102**: 10233–10237. doi:10.1073/pnas.0501062102

Gallet, R., Lenormand, T. & Wang, I.N. 2012. Phenotypic Stochasticity Protects Lytic Bacteriophage Populations From Extinction During The Bacterial Stationary Phase. *Evolution* **66**: 3485–3494. doi:10.1111/j.1558-5646.2012.01690.x

García-Villada, L. & Drake, J.W. 2013. Experimental selection reveals a trade-off between fecundity and lifespan in the coliphage Qß. *Open Biol.* **3**: 130043. doi:10.1098/rsob.130043

Garland, T.J., Dickerman, A.W., Janis, C.M. & Jones, J.A. 1993. Phylogenetic analysis of covariance by computer simulation. *Syst. Biol.* **42**: 265–292.

Garza, D.R. & Suttle, C.A. 1998. The Effect of Cyanophages on the Mortality of Synechococcus spp. and Selection for UV Resistant Viral Communities. *Microb. Ecol.* **36**: 281–292.

Goldhill, D.H. & Turner, P.E. 2014. The evolution of life history trade-offs in viruses. *Curr. Opin. Virol.* **8**: 79–84.

Graves, M.V., Bernadt, C.T., Cerny, R. & Van Etten, J.L. 2001. Molecular and genetic evidence for a virus-encoded glycosyltransferase involved in protein glycosylation. *Virology* **285**: 332–345.

Greiner, T., Frohns, F., Kang, M., Van Etten, J.L., Käsmann, A., Moroni, A., *et al.* 2009. Chlorella viruses prevent multiple infections by depolarizing the host membrane. *J. Gen. Virol.* **90**: 2033–2039.

Hall, M.D., Bento, G. & Ebert, D. 2017. The evolutionary consequences of stepwise infection processes. *Trends Ecol. Evol.* **32**: 612–623. doi:10.1016/j.tree.2017.05.009

Heineman, R.H. & Brown, S.P. 2012. Experimental Evolution of a Bacteriophage Virus Reveals the Trajectory of Adaptation across a Fecundity/Longevity Trade-Off. *PLoS One* **7**. doi:10.1371/journal.pone.0046322

Heineman, R.H. & Bull, J.J. 2007. Testing optimality with experimental evolution: Lysis time in a bacteriophage. *Evolution* **61**: 1695–1709. doi:10.1111/j.1558-5646.2007.00132.x

Hiatt, C.W. 1964. Kinetics of the inactivation of viruses. *Bacteriol. Rev.* **28**: 150–163.

Holm, S. 1979. A simple sequentially rejective multiple test procedure. *Scand. J. Stat.* **6**: 65–70.

Horas, E.L., Theodosiou, L. & Becks, L. 2018. Why Are Algal Viruses Not Always Successful? *Viruses* **10**: 474.
Hyman, P. & Abedon, S.T. 2009. Practical Methods for Determining Phage Growth Parameters. In: *Bacteriophages: Methods and Protocols, Volume 1: Isolation, Characterization, and Interactions, vol. 401* (M. R. J. Clokie & A. M. Kropinski, eds), pp. 175–202. Humana Press
Jeanniard, A., Dunigan, D.D., Gurnon, J.R., Agarkova, I. V., Kang, M., Vitek, J., *et al.* 2013. Towards defining the chloroviruses: A genomic journey through a genus of large DNA viruses. *BMC Genomics* **14**. doi:10.1186/1471-2164-14-158
Josse, J. & Husson, F. 2016. missMDA: A Package for Handling Missing Values in Multivariate Data Analysis. *J. Stat. Softw.* **70**: 1–31.
Jurczak-Kurek, A., Gąsior, T., Nejman-Faleńczyk, B., Bloch, S., Dydecka, A., Topka, G., *et al.* 2016. Biodiversity of bacteriophages: Morphological and biological properties of a large group of phages isolated from urban sewage. *Sci. Rep.* **6**: 1–17. doi:10.1038/srep34338
Kahn Mirzaei, M. & Nilsson, A.S. 2015. Isolation of Phages for Phage Therapy: A Comparison of Spot Tests and Efficiency of Plating Analyses for Determination of Host Range and Efficacy. *PLoS One* **10**: e0118557.
Kannoly, S., Oken, G., Shadan, J., Musheyev, D., Singh, K., Singh, A., *et al.* n.d. A Single-Cell Approach Reveals Variation in Cellular Phage-Producing Capacities. *bioRxiv* doi:https://doi.org/10.1101/2021.10.19.465070, doi: https://doi.org/10.1101/2021.10.19.465070
Keen, E.C. 2014. Tradeoffs in bacteriophage life histories. *Bacteriophage* **4**: e28365.
Klasse, P.J. 2015. Molecular Determinants of the Ratio of Inert to Infectious Virus Particles. *Prog. Mol. Biol. Transl. Sci.* **129**: 285–326.
Koch, G. 1960. Influence of assay conditions on infectivity of heated poliovirus. *Virology* **12**: 601–603.
Kukkaro, P. & Bamford, D.H. 2009. Virus–host interactions in environments with a wide range of ionic strengths. *Environ. Microbiol. Rep.* **1**: 71–77.
Leggett, H.C., Benmayor, R., Hodgson, D.J. & Buckling, A. 2013. Experimental evolution of adaptive phenotypic plasticity in a parasite. *Curr. Biol.* **23**: 139–142. doi:10.1016/j.cub.2012.11.045
Lippé, R. 2018. Flow Virometry: a Powerful Tool To Functionally Characterize Viruses. *J. Virol.* **92**: e01765–17. doi:10.1128/jvi.01765-17
Long, A.M. & Short, S.M. 2016. Seasonal determinations of algal virus decay rates reveal overwintering in a temperate freshwater pond. *ISME J.* **10**: 1602–1612. doi:10.1038/ismej.2015.240
Maat, D.S. & Brussaard, C.P.D. 2016. Both phosphorus- and nitrogen limitation constrain viral proliferation in marine phytoplankton. *Aquat. Microb. Ecol.* **77**: 87–97. doi:10.3354/ame01791
Meints, R.H., Burbank, D.E., Van Etten, J.L. & Lamport, D.T.A. 1988. Properties of the chlorella receptor for the virus PBCV-1. *Virology* **164**: 15–21.
Middelboe, M., Jacquet, S. & Weinbauer, M. 2008. Viruses in freshwater ecosystems: an introduction to the exploration of viruses in new aquatic habitats. *Freshw. Biol.* **53**: 1069–1075.
Milrot, E., Shimoni, E., Dadosh, T., Rechav, K., Unger, T., Van Etten, J.L., *et al.* 2017. Structural studies demonstrating a bacteriophage-like replication cycle of the eukaryote-infecting Paramecium bursaria chlorella virus-1. *PLOS Pathog.* **13**: e1006562.
Mojica, K.D.A. & Brussaard, C.P.D. 2014. Factors affecting virus dynamics and microbial host–virus interactions in marine environments. *FEMS Microbiol. Ecol.* **89**: 495–515.
Nakagawa, S. & Schielzeth, H. 2010. Repeatability for Gaussian and non-Gaussian data: a practical guide for biologists. *Biol. Rev.* **85**: 935–956.
Nichols, H.W. & Bold, H.C. 1965. Trichosarcina polymorpha Gen. et Sp. Nov. *J. Phycol.* **1**: 34–38.
Noble, R.T. & Fuhrman, J.A. 1997. Virus decay and its causes in coastal waters. *Appl. Environ. Microbiol.* **63**: 77–83. doi:10.1128/aem.63.1.77-83.1997
Pasek, J. 2021. weights: Weighting and Weighted Statistics, version 1.0.4

Pinon, A. & Vialette, M. 2018. Survival of viruses in water. *Intervirology* **61**: 214–222.
Podani, J., Kalapos, T., Barta, B. & Schmera, D. 2021. Principal component analysis of incomplete data – A simple solution to an old problem. *Ecol. Inform.* **61**: 101235. doi:10.1016/j.ecoinf.2021.101235
Quispe, C.F., Esmael, A., Sonderman, O., McQuinn, M., Agarkova, I., Battah, M., *et al.* 2017. Characterization of a New Chlorovirus Type with Permissive and Non-permissive Features on Phylogenetically Related Algal Strains. *Virology* **500**: 103–113. doi:10.1016/j.virol.2016.10.013.Evolutionary
Quispe, C.F., Sonderman, O., Seng, A., Rasmussen, B., Weber, G., Mueller, C., *et al.* 2016. Three-year survey of abundance, prevalence and genetic diversity of chlorovirus populations in a small urban lake. *Arch. Virol.* **161**: 1839–1847. doi:10.1007/s00705-016-2853-4
R Core Team. 2014. R: A language and environment for statistical computing
Rabinovitch, A., Hadas, H., Einav, M., Melamed, Z. & Zaritsky, A. 1999. Model for Bacteriophage T4 Development in Escherichia coli. *J. Bacteriol.* **181**: 1677–1683.
Record, N.R., Talmy, D. & Våge, S. 2016. Quantifying tradeoffs for marine viruses. *Front. Mar. Sci.* **3**: 251.
Refardt, D., Bergmiller, T. & Kümmerli, R. 2013. Altruism can evolve when relatedness is low: Evidence from bacteria committing suicide upon phage infection. *Proc. R. Soc. B Biol. Sci.* **280**: 20123035. doi:10.1098/rspb.2012.3035
Revell, L.J. 2012. phytools: An R package for phylogenetic comparative biology (and other things). *Methods Ecol. Evol.* **3**: 217–223.
Rodrigues, R.A.L., Queiroz, V.F., Ghosh, J., Dunigan, D.D. & Van Etten, J.L. 2022. Functional Genomic Analyses Reveal an Open Pan-genome for the Chloroviruses and a Potential for Genetic Innovation in New Isolates. *J. Virol.* **96**: e01367–21. doi:10.1128/jvi.01367-21
Rowe, J.M., Dunigan, D.D., Blanc, G., Gurnon, J.R., Xia, Y. & Van Etten, J.L. 2013. Evaluation of higher plant virus resistance genes in the green alga, Chlorella variabilis NC64A, during the early phase of infection with Paramecium bursaria chlorella virus-1. *Virology* **442**: 101–113.
Roy, D., Chian, E.S.K. & Engelbrecht, R.S. 1982. Mathematical model for enterovirus inactivation by ozone. *Water Res.* **16**: 667–673.
Schiano di Visconte, G., Allen, M.J. & Spicer, A. 2022. New Insights from the High-Resolution Monitoring of Microalgae–Virus Infection Dynamics. *Viruses* **14**: 466.
Stearns, S.C. 1989. Trade-Offs in Life-History Evolution. *Funct. Ecol.* **3**: 259–268.
Stenholm, A.R., Dalsgaard, I. & Middelboe, M. 2008. Isolation and Characterization of Bacteriophages Infecting the Fish Pathogen Flavobacterium psychrophilum. *Appl. Environ. Microbiol.* **74**: 4070–4078.
Šulčius, S., Šimoliūnas, E., Staniulis, J., Koreivienė, J., Baltrušis, P., Meškys, R., *et al.* 2015. Characterization of a lytic cyanophage that infects the bloom-forming cyanobacterium Aphanizomenon flos-aquae. *FEMS Microbiol. Ecol.* **91**: 1–7.
Suttle, C.A. 2007. Marine viruses - Major players in the global ecosystem. *Nat. Rev. Microbiol.* **5**: 801–812.
Suttle, C.A. & Chan, A.M. 1994. Dynamics and distribution of cyanophages and their effect on marine Synechococcus spp. *Appl. Environ. Microbiol.* **60**: 3167–3174. doi:10.1128/aem.60.9.3167-3174.1994
Swihart, B. & Lindsey, J. 2019. gnlm: Generalized Nonlinear Regression Models, version 1.1.1
Taylor, B.P., Weitz, J.S., Brussaard, C.P.D. & Fischer, M.G. 2018. Quantitative Infection Dynamics of Cafeteria Roenbergensis Virus. *Viruses* **10**: 468.
Thiel, G., Moroni, A., Dunigan, D.D. & Van Etten, J.L. 2010. Initial Events Associated with Virus PBCV-1 Infection of Chlorella NC64A. *Prog. Bot.* **71**: 169–183.
Timm, A. & Yin, J. 2012. Kinetics of virus production from single cells. *Virology* **424**: 11–17.
Tomaru, Y., Tanabe, H., Yamanaka, S. & Nagasaki, K. 2005. Effects of temperature and light on stability of microalgal viruses, HaV, HcV and HcRNAV. *Plankt. Biol. Ecol.* **52**: 1–6.

Tseng, M. & Myers, J.H. 2014. The relationship between parasite fitness and host condition in an insect -virus system. *PLoS One* **9**: e106401. doi:10.1371/journal.pone.0106401
Van Etten, J.L., Agarkova, I. & Dunigan, D.D. 2020. Chloroviruses. *Viruses* **12**: 20.
Van Etten, J.L., Burbank, D.E., Xia, Y. & Meints, R.H. 1983. Growth cycle of a virus, PBCV-1, that infects Chlorella-like algae. *Virology* **126**: 117–125.
Van Etten, J.L., Schuster, A.M. & Meints, R.H. 1988. Viruses of eukaryotic Chlorella-like algae. In: *Viruses of Fungi and Simple Eukaryotes* (Y. Koltin & M. J. Leibowitz, eds), pp. 411–428. New York and Basel
Vincent, F., Sheyn, U., Porat, Z., Schatz, D. & Vardi, A. 2021. Visualizing active viral infection reveals diverse cell fates in synchronized algal bloom demise. *Proc. Natl. Acad. Sci. U. S. A.* **118**: e2021586118.
Weitz, J. 2016. *Quantitative Viral Ecology: Dynamics of Viruses and Their Microbial Hosts*. Princeton University Press
Wen, K., Ortmann, A.C. & Suttle, C.A. 2004. Accurate estimation of viral abundance by epifluorescence microscopy. *Appl. Environ. Microbiol.* **70**: 3862–3867. doi:10.1128/AEM.70.7.3862-3867.2004
Williamson, K.E., Fuhrmann, J.J., Wommack, K.E. & Radosevich, M. 2017. Viruses in Soil Ecosystems: An Unknown Quantity Within an Unexplored Territory. *Annu. Rev. Virol.* **4**: 201–19.
Yan, X., Olson, N.H., Van Etten, J.L., Bergoin, M., Rossmann, M.G. & Baker, T.S. 2000. Structure and assembly of large lipid-containing dsDNA viruses. *Nat. Struct. Biol.* **7**: 101–103.
Zera, A.J. & Harshman, L.G. 2001. The Physiology of Life History Trade-Offs in Animals. *Annu. Rev. Ecol. Syst.* **32**: 95–126.

Tables

Table 1. Definitions used in this paper.

Term	Our definition	Concentration measured by	Ratio to host cells
Virions	All virus particles.	Flow cytometry.	Multiplicity of particles (MOP)
Adsorbed virions	Virions that are adsorbed to a host cell.	-	Multiplicity of adsorption (MOA)[1]
Depolarizing-capable virions	Virions that can depolarize a host cell if they adsorb to one. Depolarization leads to DNA entry and exclusion of any other depolarizing-capable virions that may adsorb[2].	-	-
Infective virions	Virions that can catalyze the death of an algal population. We assume that these are virions that can finish a life cycle (i.e. successfully adsorb, depolarize, complete lysis, and release progeny).	Mixing algae and viruses at different virus dilutions and monitoring host death. This is analogous to a most probable number assay or plaque assay.	Multiplicity of infection (MOI)

[1]following (Hyman & Abedon, 2009), [2](Greiner *et al.*, 2009)

Table 2. List of viral strains. We used two lysates of reference strain AR158; lysate AR158[1] was seven years older than AR158[2]. Phylogenetic positions are based on Quispe et al. (2017) and Rodrigues et al. (Rodrigues *et al.*, 2022).

Group	Clade	Strains
NC64A viruses	PBCV-1 clade	AN69C, CV-K1 (= CviKI), CvsA1, IL-3A, KS-1B, MA-1E, NE-JV-4, PBCV-1
	NY-2A clade	AR158[1], AR158[2], IL-5-2s1, MA-1D, NY-2A, NY-2B, NYs-1
	unknown	CA-4A, SH-6A, WNE-10B-L2, WNE-11A-L2 (= WNE-11A-L1), XZ-4A
Osy viruses	Osy clade	OSyNE-5
	unknown	OSyNE-4B-L2, OSyNE-4B-M2, OSyNE-4B-S2, OSyNE-5B-M2, OSyNE-5B-S1, OSyNE-ZA-1
SAG viruses	SAG clade	Canal-1, GM0701.1, MN0810.1, MO0605SPH, NTS-1, TN603.4.2
	unknown	NES-4A-S1, NES-5A-L1

Table 3. Additional correlations that we hypothesized could occur between traits, based on trade-offs found in or suggested by the literature.

Trade-off	Expected trait correlations	Basis
Short-term vs. long-term virion quality	- specific infectivity *s* positively correlated with decay rate *m* - specific infectivity *s* negatively correlated with the robust fraction *r*	Reflection of the general expectation that trade-offs occur between adaptations to different environments (Agrawal *et al.*, 2010), in this case short-term and long-term outside-host conditions.
Survival vs. reproduction	- decay rate *m* positively correlated with multiplication rate, which we calculate as b_c*s/μ_l to match (De Paepe & Taddei, 2006) - decay rate *m* positively correlated with relative growth in the growth assay	General review in (Stearns, 1989); discussed for viruses in (Goldhill & Turner, 2014; Keen, 2014). Seminal example in(De Paepe & Taddei, 2006).
Offspring quantity & quality	- burst size per infected cell b_d negatively correlated with specific infectivity *s*	Version of the quantity/quality trade-off discussed in (Stearns, 1989; Keen, 2014), but at $t = 0$. Related to the speed-fidelity trade-off (Furió *et al.*, 2005; Belshaw *et al.*, 2008), though other processes than mutation may cause defective virions.

Figures

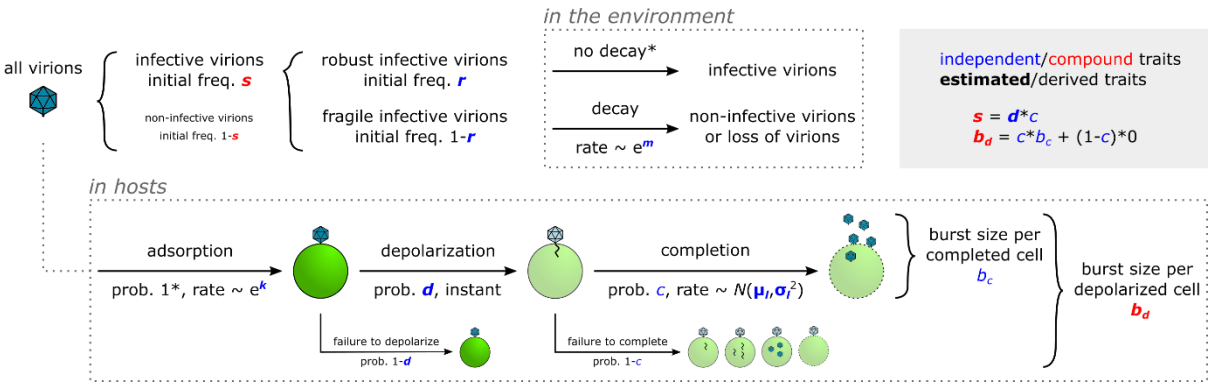

Figure 1. Life cycle of the chloroviruses, as assumed in our statistical models. See the text for explanations and definitions of the traits. Traits marked in blue are assumed to be independent of each other; traits marked in red arise from combinations of two or more other traits. Traits in bold are estimated from the mOSG or mP assay results; traits not in bold are derived from comparing the two assays. We make the assumptions (*) that the traits are independent of each other, that all virions can adsorb, and that robust infective virions do not decay; these assumptions are not contradicted by our data but may need to be revised in further work.

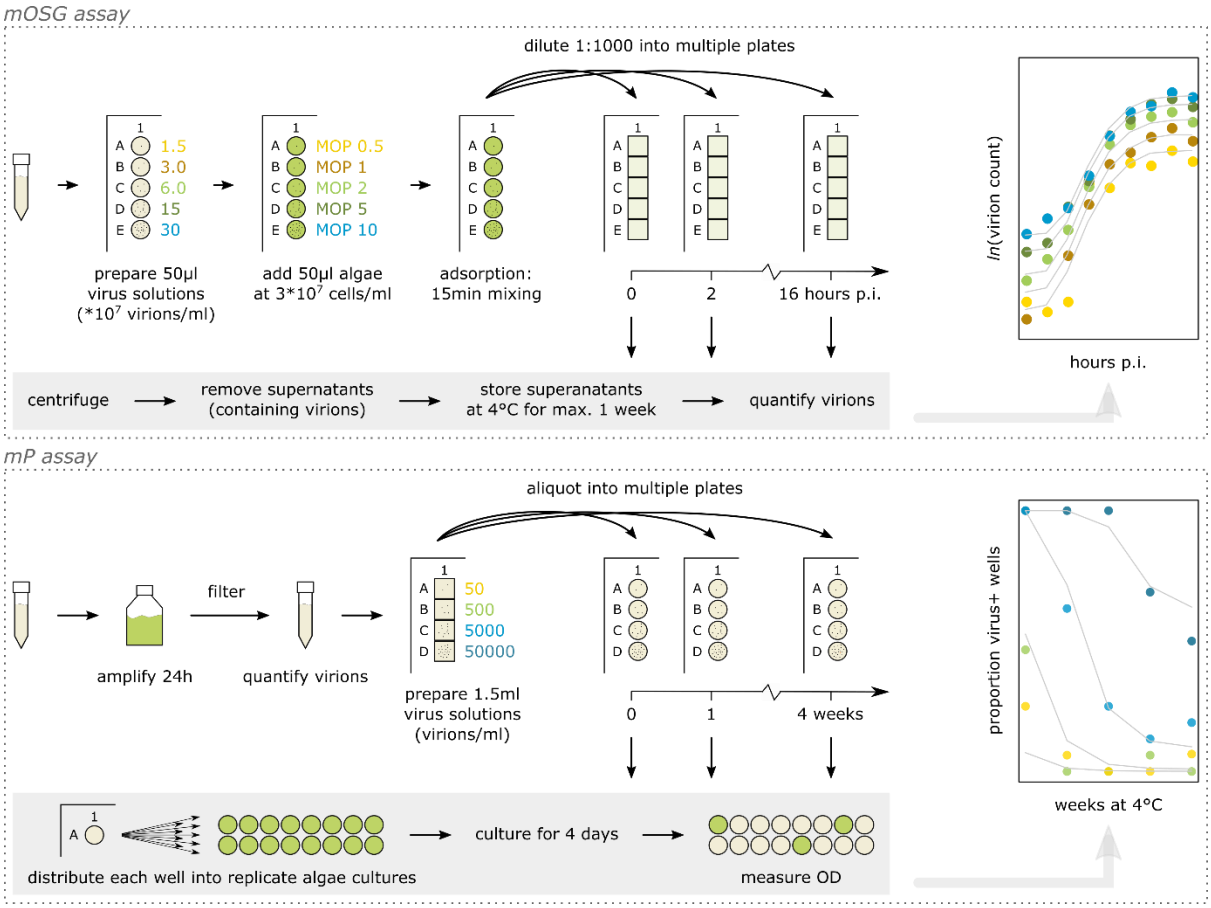

Figure 2. Schematic representation of the mOSG and mP assays for one virus strain. Both assays started from the same filtrate, represented by a 15ml tube. Culture plates are depicted with round wells; deep well plates with square wells. The solid gray boxes describe the sampling procedure that was repeated at every time point. On the right, the gray arrows lead to examples of the data (points) and the model fits (gray lines). The data shown here is for virus SH-6A.

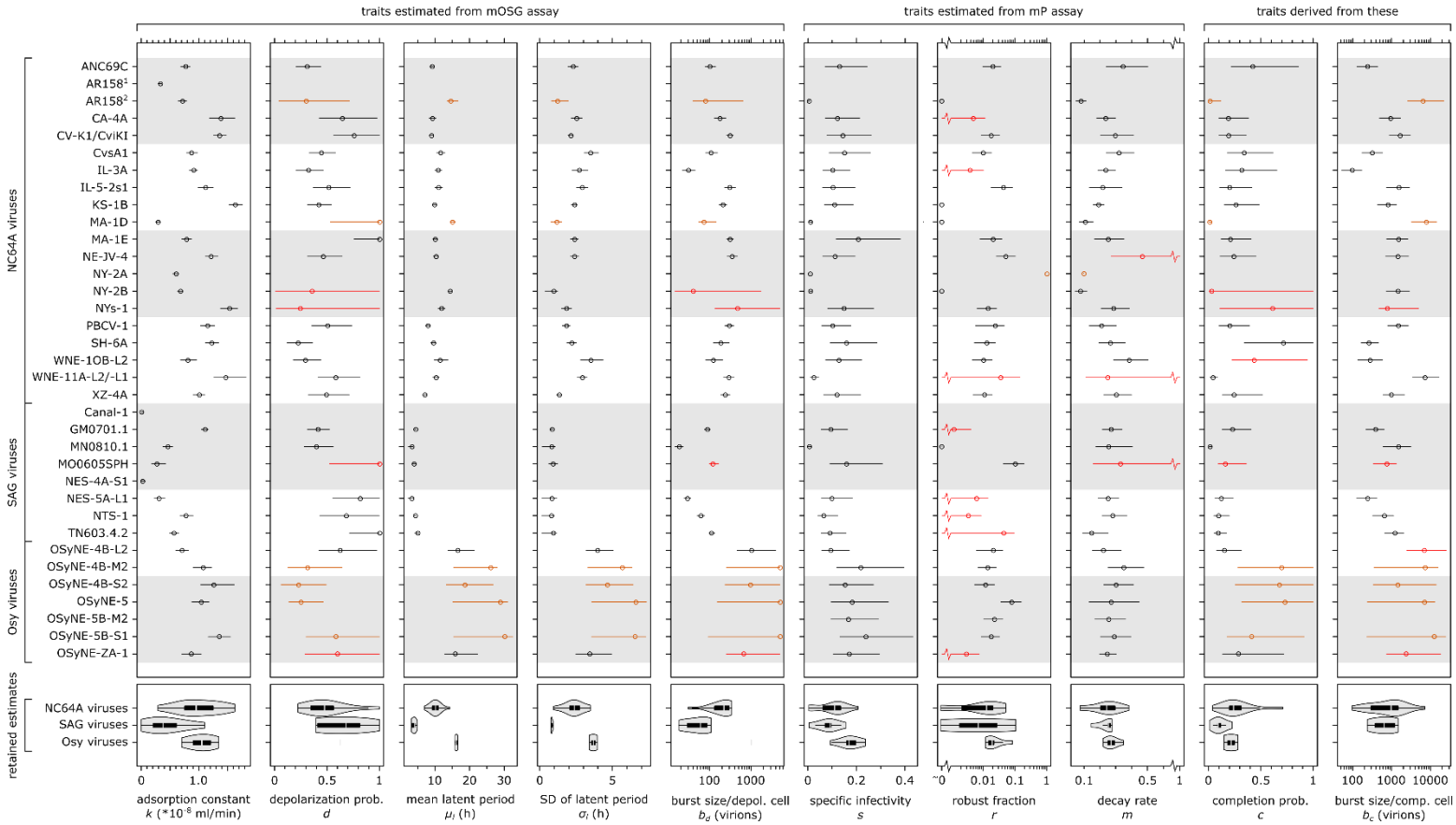

Figure 3. Within- and across-group trait diversity revealed by the mOSG and mP assays. Upper panels: Trait estimates and 95% CIs. Missing traits are due to assay failures (e.g. the strain did not grow within the time of the mOSG assay, or did not infect at all in the mP assay). Traits and CIs marked in orange were excluded from the analyses because the assay was incomplete (e.g. the strain was still growing at the end of the mOSG assay, or there was no decay in the mP assay). Traits derived from these are also marked in orange and were excluded from the analyses. Finally, traits and CIs marked in red were excluded from the analyses because the models fit poorly or because the CI was so broad as to render the estimate uninformative (CI criteria were: CI > 0.67 for *d*, *s*, and *c*; CI spanning more than an order of magnitude for b_d, *r*, and b_c; CI overlapping with the upper fitting constraint for *k*, μ_l, σ_l, and *m*). See Supp. Table 1 for exact values of the estimates and CIs used in the analyses. **Lower panels: Distributions of the retained estimates.** Shown as violin plots with internal box plots. Only the estimates used in the analyses are included in these distributions (i.e. those shown in black in the upper panels).

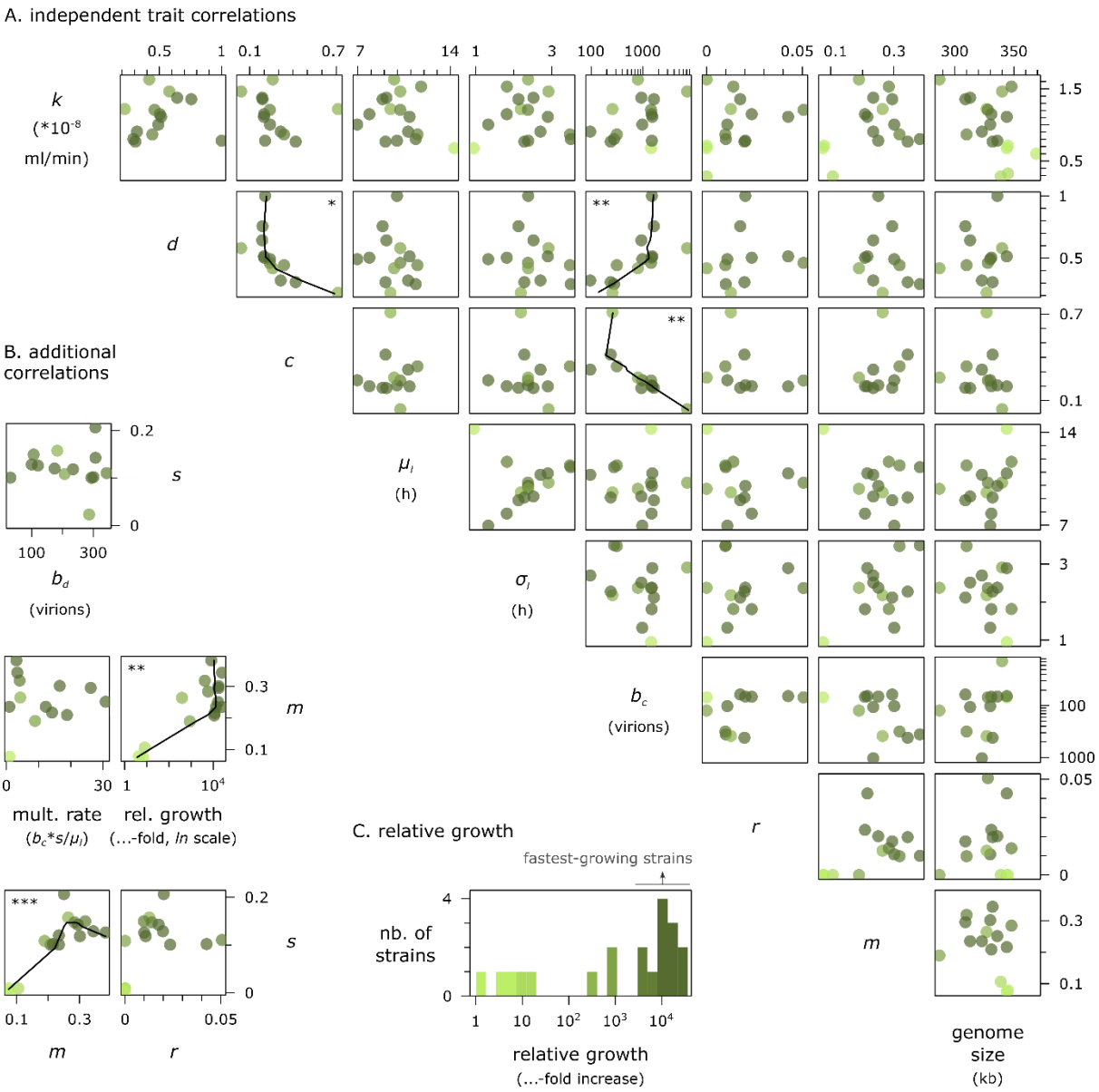

Figure 4. Correlations between traits in the NC64A viruses. Shade represents high (dark green) vs. low (light green) relative growth in the growth assay (see panel C). **A.** Pairwise correlations between independent traits. **B.** Additional correlations that we hypothesized might occur ("mult. rate" multiplication rate; "rel. growth" relative growth). **A&B.** Each point represents one virus strain. Significant correlations are marked with stars and fitted with LOESS curves. Note that the analyses were weighted by the precision of the retained estimates, and this weighting is not represented in the figure. **C.** Results of the growth assay, expressed as an x-fold increase in virion concentration in 24h. The 12 fastest-growing strains are marked.

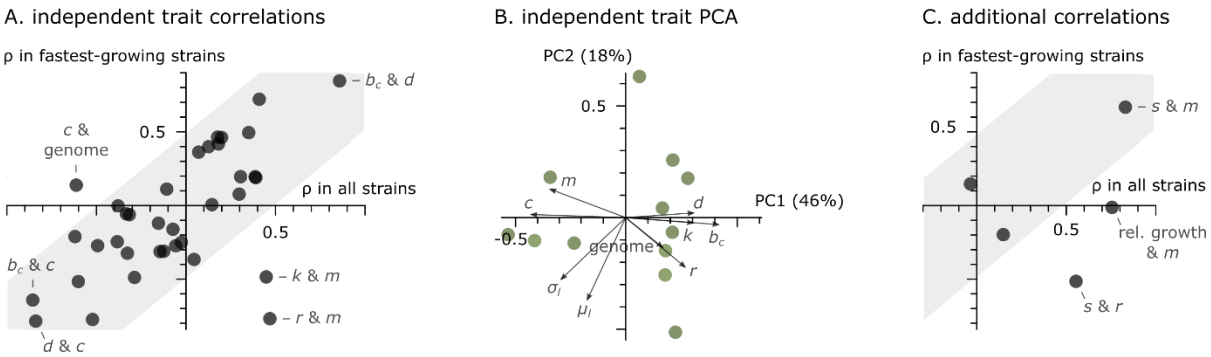

Figure 5. Correlations between traits in the fastest-growing NC64A viruses. The fastest-growing NC64A viruses are marked in Fig. 4C. **A&C.** Comparison of Spearman's ρ correlation coefficients between independent traits (**A**) or for additional trait combinations (**C**) when all strains (cf. Fig. 4A resp. 4B) vs. the fastest-growing strains are used. Each point represents one combination of traits. The gray area marks the zone where $-0.5 \leq \Delta\rho \leq 0.5$; points outside this zone are marked with the trait combination they represent. **B.** PCA of the independent traits in the fastest-growing strains. The biplot shown here was produced by the Ipca method; the PairCor result was extremely similar. The variance explained by each principal component (PC) is given on the axis. Each point represents one virus strain.

Supplementary Material

Supplementary Method 1. Protocol for virion concentration by flow cytometry. A detailed protocol is provided, along with notes on sample storage.

Supplementary Table 1. Trait table for the chloroviruses, including selected traits from the literature and the traits estimated in this manuscript. Further details provided in the file.

Supplementary Table 2. ANOVA tables partitioning the trait variance within and among chlorovirus groups. Further details provided in the file.

Supplementary Table 3. Correlations between traits in the NC64A virus group. Further details provided in the file.

Supplementary Figure 1. Example of statistical fitting for the mOSG assay. The graph at the top left shows the data with outliers removed (yellow: MOP 0.5, orange: MOP 1, light green: MOP 2, dark green: MOP 5, blue: MOP 10, indigo: MOP 20), the model fit (black lines), and the estimated parameters from Eq. 1.4 (text*). The graph at the top right is the comparison of the virus outputs at 16h for the 1:1000 and 1:10000 dilutions (the black line is the expectation if released virions do not start secondary infections). The remaining graphs are used to assess model fit: 'f' are the fitted values and 'r' are the residuals.
*The depolarization probability *d* was called *i* when this algorithm was run.

Supplementary Figure 2. Example of statistical fitting for the mP assay. The graph at the top left shows the data with outliers removed (yellow: 50 virions/ml, light green: 500 virions/ml, blue: 5000 virions/ml, indigo: 50000 virions/ml), the model fit of Eq. 7 (gray lines), the model fit of Eq. 8 (black lines), and the estimated parameters from Eq. 8 (text*). The remaining graphs are used to assess model fit: 'f' are the fitted values and 'r' are the residuals (we do not expect the residuals to be normally distributed here, as the data is binomial with limited replication).
*The decay rate *m* was called *d* and the robust fraction *r* was called *h* when this algorithm was run.

Supplementary Figure 3. Derivation of the independent traits *c* and b_c. The top row represents the derivation of *c*: it is dependent on the estimates of *s* and *d* (left graph); $c = s/d$ leads to a given relationship between *c* and *s* (middle) and *c* and *d* (right). The bottom row represents the derivation of b_c: it is dependent on the estimates of b_d and *c* (left graph); $b_c = b_d/c$ leads to a given relationship between b_c and b_d (middle) and b_c and *c* (right). Each point represents one virus strain. Colors represent the NC64A viruses (green), SAG viruses (blue), and Osy viruses (brown). Shade represents high (dark) vs. low (light) relative growth in the growth assay. Lines represent 95% CIs around each estimate.

Supplementary Figure 4. Amplitude~MOP of mOSG curves if burst size is constant. In our mOSG analysis models, we assumed that the parameters were independent of MOP, and therefore that the amplitude of mOSG curves saturates with MOP: as MOP increases, the proportion of depolarized algal cells approaches 1 (following a Poisson probability function with rate *d*MOA*, see Eqs. 3-5), and the number of new virions after lysis approaches a maximum. We investigated whether this was the case for every virus strain whose estimates of *d* and b_d were retained. It was done in three steps:
1) First, we fit a model that to the mOSG data did not assume independent depolarization probability, lysis time, or burst size per depolarized cell. This model, $V(t) = \frac{1}{\delta} * \left(A_{ads} * MOP * e^{-k*A_{ads}*t_{ads}} + A_{ads} * CDF(t, \mu_l[MOP], \sigma_l[MOP]) * \alpha[MOP]\right)$, fit a separate latent period (μ_l, σ_l) and amplitude (α) to each MOP curve, but a joint adsorption rate *k*. The amplitude is the difference between the virion concentration after complete lysis and the concentration of unadsorbed virions

(determined by *k*); it can be seen as the product of the proportion of depolarized cells and the burst size per depolarized cell. An example is shown in **panel A**. The statistical fitting was done as for Eq. 1.4.

2) Next, we checked whether the amplitudes saturated as expected under the assumption of MOP-independence, i.e. under the Poisson probability model $\alpha = \left(1 - e^{-d*\left(1-e^{-k*A_{ads}*t_{ads}}\right)*MOP}\right) * b_d$. We fit this model to the absolute and *ln*-transformed amplitude data, then evaluated the fit of the predicted curves (an example is shown in **panels B&C**). We generally found a close correspondence between the two, suggesting that the burst size is independent of MOP. The statistical fitting was done as for Eq. 1.4, though without imposing upper and lower bounds on the parameters and using both the absolute and *ln*-transformed scales. (The difference between doing steps (1+2) and simply fitting Eq. 1.4 is that this procedure does not assume that lysis time is independent of MOP, and thus makes fewer assumptions.)

3) We investigated how sensitive step (2) was to deviations from independence. Note that this investigation was a proof of concept rather than a thorough power analysis. First, we generated two sets of artificial mOSG assay data. We predicted data using the strain's estimated traits and Eq. 1.4, but set b_d to be 1.5 times *i*) higher or *ii*) lower at MOPs 5 and 10. This artificially increased and decreased the amplitudes of the mOSG curves for MOP 5 and 10. We then added realistic residuals, namely the residuals of the true data. Examples are shown in the **panel D** (1.5x higher) and **panel G** (1.5x lower): circles indicate the true data, crosses indicate the artificial data. We then ran steps (1) and (2) on the artificial datasets (fitted lines in the **panels D & G**, amplitude~MOP models in **panels E-F and H-I**), and compared their log-likelihood (i.e. their fit) with that of the true data. **Panels J and K** show the results of these comparisons. In many cases, there is no clear difference between the fit of the Poisson probability model for the true and the artificial data. This leads us to conclude that while our data does not conflict with the assumption of constant burst size, we have limited power to detect deviations from it.